ELSEVIER

Chemical Geology 167 (2000) 285–312

CHEMICAL GEOLOGY
INCLUDING
ISOTOPE GEOSCIENCE

www.elsevier.com/locate/chemgeo

# The effects of K-metasomatism on the mineralogy and geochemistry of silicic ignimbrites near Socorro, New Mexico

D.J. Ennis [a,b], N.W. Dunbar [a,c,*], A.R. Campbell [a], C.E. Chapin [c]

[a] *Department of Earth and Environmental Science, New Mexico Institute of Mining and Technology, Socorro, NM 87801, USA*
[b] *RAMCO Environmental 2065-G Sperry Ave., Ventura, CA 93003, USA*
[c] *New Mexico Bureau of Mines and Mineral Resources, New Mexico Institute of Mining and Technology, Socorro, NM 87801, USA*

Received 8 December 1998; accepted 9 November 1999

**Abstract**

K-metasomatism of the upper Lemitar and Hells Mesa silicic ignimbrites near Socorro, New Mexico is thought to be the result of downward percolation of alkaline, saline brines in a hydrologically closed basin [Chapin, C.E., Lindley, J.I., 1986. Potassium metasomatism of igneous and sedimentary rocks in detachment terranes and other sedimentary basins: economic implications. Arizona Geological Society Digest, XVI, 118–126.]. During the chemical changes associated with metasomatism, Na-rich phases, primarily plagioclase, are replaced by secondary mineral phases. Adularia, a low-temperature K-feldspar, is the dominant mineral formed during K-metasomatic alteration, but mixed-layer I/S, discrete smectite, and kaolinite can also be present in the assemblage. The formation of discrete smectite within the assemblage during K-metasomatism may have occurred during periods of low cation/$H^+$ ratios in the alkaline, saline brine. Upon an increase in the cation/$H^+$ ratio, such as could occur during evaporation of the alkaline lake, the solution may have become sufficiently concentrated to cause illitization of smectite resulting in the formation of mixed-layer I/S within the assemblage. Distribution of phases in the alteration assemblage strongly suggests a dissolution–precipitation reaction for K-metasomatism in the Socorro area as indicated by the presence of dissolution embayments in plagioclase crystals, the presence of euhedral adularia, and the common occurrence of authigenic clay minerals in the assemblage. K-metasomatism causes significant chemical modification of the silicic ignimbrite, particularly increases in $K_2O$ and Rb and depletion of $Na_2O$ and Sr with increasing adularia abundance. The correlation between Rb and $K_2O$ suggests that Rb is enriched during alteration due to substitution for K in adularia. The effect of hydrothermal activity, either prior to, or following metasomatism, is also observed in some samples, as shown by high concentrations of elements such as Ba, As, Sb, Pb and Cs.

Enrichment of middle and HREE in the upper Lemitar Tuff samples and depletion of middle and HREE in Hells Mesa Tuff samples suggests attempted re-equilibration between the secondary alteration assemblage and the metasomatizing fluid. Preliminary data indicate clay minerals within the secondary assemblage may have played an important role in the incorporation of REE during redistribution. 

## 1. Introduction

A number of areas of the western United States, particularly areas of basin and range extension, are

* Corresponding author.
*E-mail address:* nelia@nmt.edu (N.W. Dunbar).

0009-2541/00/$ - see front matter 
PII: S0009-2541(99)00223-5

characterized by rocks that have been secondarily enriched in potassium (K) (Duval, 1990). Many of these areas, including the Socorro, New Mexico area, are hypothesized to be caused by K-metasomatism (Chapin and Lindley, 1986), a secondary alteration process caused by interaction between a K-rich fluid and the host rock. During K-metasomatism some elements, such as K, become concentrated in the altered rock, whereas other elements become depleted. In some cases, the altered rocks are significantly enriched in elements of economic interest (Chapin and Lindley, 1986; Dunbar et al., 1994). Therefore, it is important to understand the process by which K-metasomatism occurs, and the origin of the chemical and mineralogical alteration. The fluids that cause K-metasomatism may be derived from a number of sources including; magmatic (Shafiqullah et al., 1976; Rehrig et al., 1980); hydrogen metasomatized basement rocks from deep within a metamorphic complex (Glazner, 1988); or from low-temperature alkaline, saline aqueous systems within a hydrologically closed basins (Chapin and Lindley, 1986; Turner and Fishman, 1991; Leising et al., 1995).

The aim of this study is to investigate the mineralogical and chemical alteration within two rhyolitic ignimbrite sheets, the upper Lemitar and Hells Mesa Tuffs, as a function of intermediate to advanced degrees of K-metasomatism. Specifically, the objective is to study the mobility of major and trace elements with respect to the alteration mineral assemblage formed during K-metasomatism.

### *1.1. Background*

Many areas that have undergone regional crustal extension show evidence of K-metasomatism of volcanic and sedimentary rocks along regional, low-angle normal faults or 'detachment faults' (Davis et al., 1986). Evidence for K-metasomatism associated with regional extension is reported by Brooks (1986) at Picacho Peak, Roddy et al. (1988) in the Harcuvar Mountains in Arizona, and by Glazner (1988) in the Sleeping Beauty area, Central Mojave Desert.

The K-anomaly near Socorro, New Mexico is located in the northeast corner of the Mogollon–Datil volcanic field and is approximately L-shaped with an area of roughly 40–50 km on a side and 20 km in width (Fig. 1). The area contains a sequence, oldest to youngest, of five silicic ignimbrites interbedded with mafic lava flows: Hells Mesa, La Jencia, Vicks Peak, Lemitar, and South Canyon Tuffs. Together, the stratigraphic thickness of the tuffs is approximately 500 m in the Socorro area, and the ages range from Oligocene to early Miocene (Chapin and Lindley, 1986). Both the upper Lemitar and Hells Mesa Tuffs are present both within and outside the zone of K-metasomatic alteration thereby allowing for the sampling and examination of both altered and unaltered rocks. The volcanic stratigraphy in the Socorro area is extensively faulted and offset. As a result of this structural complexity, the Hells Mesa and Lemitar Tuffs are present at a variety of elevations, and during an alteration event would have been exposed to a range of fluid compositions. Variable degrees of alteration are also present within each of the other ignimbrite units.

Based on a number of factors, Chapin and Lindley (1986) interpret the Socorro K-anomaly to be the result of widespread alteration by alkaline, saline water derived from a large playa lake. First, the large aerial extent affected by K-alteration is difficult to explain as a result of hydrothermal alteration. Although localized areas of hydrothermal activity are known to exist in the Socorro K-anomaly, a magmatic system of the magnitude necessary to cause such a large alteration is not known to have existed in the time frame when K-metasomatism was thought to be active. Based on $^{40}Ar/^{39}Ar$ radiometric dating, K-metasomatism is confirmed to have been active between 8.7 and 7.4 Ma, but possibly started as early as 15 Ma (Dunbar et al., 1994, 1996). In addition, the K-metasomatized rocks in the Socorro area are enriched in $\delta^{18}O$ (Chapin and Lindley, 1986; Dunbar et al., 1994), which is not indicative of fluids associated with a high-temperature magmatic system. Lastly, the presence of thick playa deposits in the Socorro area suggest the occurrence of a long-lived evaporative lacustrine environment, possibly of evolving alkaline–saline waters. Once the closed lacustrine environment was established, the metasomatizing fluids may have been transported by vertical advection caused by salinity-induced density stratification (Leising et al., 1995). A similar mechanism was invoked for K-alteration of tuffaceous rocks in the Green River Formation of Wyoming (Surdam and Parker, 1972).

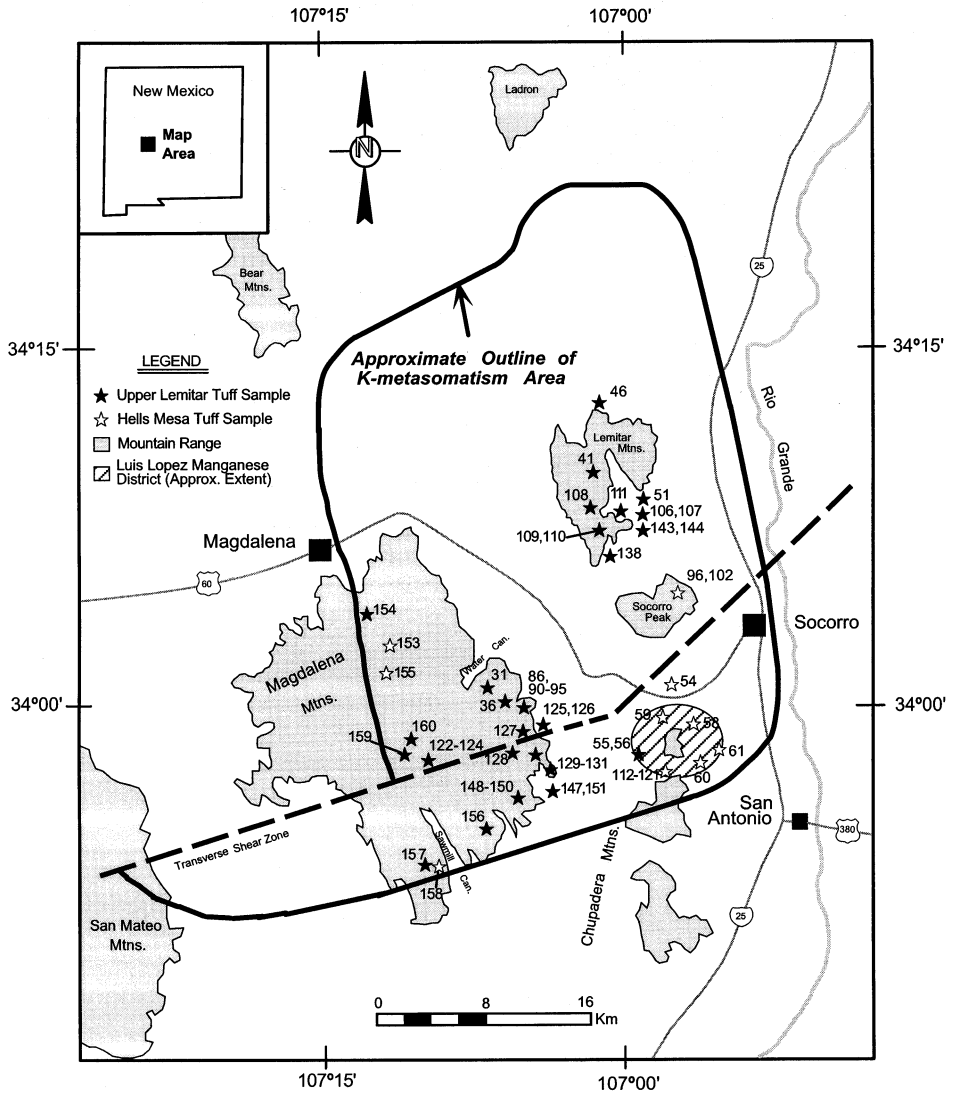


Fig. 1. Map of the Socorro K-metasomatized area after Lindley (1979). Samples numbered with a hyphen are inclusive, i.e., 112 through 121. Stippled portions of the map represent mountains, while the white portions represent alluvial basins with limited outcrop.

The alteration process involves the selective replacement of plagioclase and other K-poor phases to produce mineral assemblages of K-feldspar (adularia) + hematite + quartz ± clay minerals (Lindley, 1985). Rocks affected by K-metasomatism commonly have a characteristic red–brown color due to hematite from the oxidation of groundmass magnetite (Lindley, 1985). $K_2O$ contents are as high as 13.5 wt.%, whereas $Na_2O$, CaO and MgO are typically each depleted to 1 wt.% or less (Chapin and Lindley, 1986). Increases in Rb and Ba along with decreases in Sr, MnO and MgO are also recognized (Chapin and Lindley, 1986).

Several localized hydrothermal systems overprint the Socorro K-metasomatic alteration including the Luis Lopez manganese district (Northern Chupadera mountains), Socorro Peak district, and the Lemitar and Magdalena Mountains districts. Psilomelane is the primary manganese phase in the Luis Lopez district and is typically associated with gangue min-

erals of calcite, hematite, and quartz with minor barite and fluorite (Norman et al., 1983). Structural evidence suggests the manganese was deposited between 7 and 3 Ma (Chamberlin, 1980; Eggleston et al., 1983) as open-space fillings in fault breccias and fault openings (Norman et al., 1983). The hydrothermal alteration associated with the Luis Lopez manganese district is younger than the K-metasomatic event and is superimposed on the regional K-anomaly (Eggleston et al., 1983; Norman et al., 1983). The host rocks in the northern portion of the Luis Lopez manganese district are the upper and lower members of the Lemitar Tuff, while the Hells Mesa Tuff is the host rock in the southern portion of the district (Eggleston et al., 1983).

### *1.1.1. Lemitar and Hells Mesa Tuffs*

The Lemitar Tuff was emplaced at $28 \pm 0.08$ Ma (McIntosh et al., 1990) and is a multiple-flow, compositionally zoned, rhyolitic ignimbrite (Chapin et al., 1978) consisting of two members. The upper member of the Lemitar Tuff is particularly crystal-rich and contains abundant plagioclase, a phase that is strongly altered during metasomatism. The upper Lemitar Tuff contains 30–35% phenocrysts and plagioclase averages between 10% and 15% of the total phenocrysts present (Osburn, 1978). The basal portion of the upper Lemitar contains between 5% to 10% plagioclase phenocrysts. Quartz and biotite along with minor amounts of magnetite, clinopyroxene, sphene, and zircon are also found within the upper member (D'Andrea, 1981).

The Hells Mesa Tuff was emplaced at $32.06 \pm 0.10$ Ma (McIntosh et al., 1990). It is a crystal-rich, densely welded, simple cooling unit containing 35% to 45% phenocrysts. Sanidine represents 10% to 30% of the total phenocryst percentage. Plagioclase averages between 8% and 30% of the total phenocrysts present (Osburn, 1978). Sub-angular quartz along with minor to trace quantities of biotite, clinopyrox-

Table 1
Relative percentages of minerals in the alteration assemblage
Percentages are estimated using ratios of peak area from XRD patterns. Sm = smectite, Mx = mixed layer illite–smectite, I = illite, K = kaolinite, N/A = not applicable due to absence of clay. 'Not determined' indicates that clay is present in the alteration assemblage however, semi-quantitative analysis was not able to be performed on that sample due to flocculation.

| Sample # | % Adularia | % Plagioclase | % Clay | Clay (parts per 10) | Sample # | % Adularia | % Plagioclase | % Clay | Clay (parts per 10) |
|---|---|---|---|---|---|---|---|---|---|
| KM-36[a] | 67 | 0 | 33 | Mx = 6, Sm = 3, I = 1 | KM-113 | 50 | 0 | 50 | K = 10 |
| KM-41 | 78 | 11 | 11 | K = 10 | KM-114 | 75 | 0 | 25 | K = 10 |
| KM-46[a] | 33 | 67 | 0 | N/A | KM-115 | 67 | 0 | 33 | K = 10 |
| KM-51[a] | 50 | 0 | 50 | Sm = 10 | KM-116 | 50 | 25 | 25 | K = 9, Mx = 1 |
| KM-54 | 50 | 0 | 50 | Mx = 8, Sm = 1, K = 1 | KM-127 | 86 | 0 | 14 | K = 10 |
| KM-55 | 89 | 0 | 11 | Mx = 9, I = 1 | KM-128 | 67 | 0 | 33 | K = 7, Mx = 2, Sm = 1 |
| KM-56 | 91 | 0 | 9 | Mx = 10 | KM-129 | 50 | 50 | 0 | N/A |
| KM-58 | 67 | 0 | 33 | K = 9, Mx = 1 | KM-131 | 25 | 50 | 25 | not determined |
| KM-59 | 50 | 0 | 50 | K = 10 | KM-144 | 89 | 0 | 11 | Mx = 7, K = 2, Sm = 1 |
| KM-60 | 29 | 14 | 57 | K = 9, I = 1 | KM-148 | 20 | 80 | 0 | N/A |
| KM-61[a] | 25 | 25 | 50 | K = 7, Sm = 3 | KM-149 | 33 | 67 | 0 | N/A |
| KM-86 | 75 | 0 | 25 | K = 9, Mx = 1 | KM-150 | 25 | 75 | 0 | N/A |
| KM-90 | 83 | 0 | 17 | not determined | KM-153 | 100 | 0 | 0 | N/A |
| KM-91 | 29 | 14 | 57 | not determined | KM-154 | 75 | 0 | 25 | Mx = 7, I = 3 |
| KM-94 | 33 | 0 | 67 | Mx = 7, I = 2, Sm = 1 | KM-155 | 33 | 0 | 67 | I = 5, Mx = 4, K = 1 |
| KM-95 | 86 | 0 | 14 | K = 7, Mx = 3 | KM-156 | 100 | 0 | 0 | N/A |
| KM-96[a] | 50 | 0 | 50 | Mx = 6, I = 4 | KM-157 | 12 | 38 | 50 | K = 6, Sm = 4 |
| KM-102 | 67 | 0 | 33 | Mx = 7, I = 3 | KM-158 | 57 | 29 | 14 | K = 6, Sm = 4 |
| KM-107 | 80 | 20 | 0 | N/A | KM-159 | 83 | 0 | 17 | I = 5, Mx = 5 |
| KM-111[a] | 55 | 27 | 18 | Sm = 9, Mx = 1 | KM-160 | 75 | 0 | 25 | I = 5, Mx = 5 |
| KM-112 | 75 | 0 | 25 | K = 10 | | | | | |

[a] Indicates samples examined by SEM.

ene, sphene, and lithic fragments are also present within the Hells Mesa Tuff (D'Andrea, 1981).

Although the geochemical composition of neither tuff has been investigated in detail, both appears to exhibit some compositional zonation. The Hells Mesa tuff ranges from rhyolitic to quartz latitic composition and is reversibly zoned with a more mafic, quartz-poor base grading into a more silicic, quartz-rich upper portion (Chapin et al., 1978). There also appears to be some compositional zonation within the upper member of the Lemitar Tuff, resulting in a distinct chemical gradation, particularly within the major elements. As will be discussed later in the paper, the major element composition of the two tuffs are very similar, although the trace elements, particular the rare earth elements, are distinctly different.

### *1.2. Sampling and analytical methods*

#### *1.2.1. Sampling and sample preparation*

The Hells Mesa and upper Lemitar Tuffs were sampled at a number of locations across the K-anomaly (Fig. 1). Some areas within the K-anomaly, however, could not be sampled due to basin fill. Sixty-three samples were collected, ranging in degree of alteration from nearly pristine to highly metasomatized. When feasible, altered plagioclase was carefully hand-picked or drilled out from the interior of former plagioclase phenocrysts using a Foredom hand drill in order to directly evaluate the mineralogy produced during K-metasomatism. Four unmetasomatized samples, two from each tuff unit, were examined in thin section in order to assess the degree to which plagioclase has been altered through processes other than K-metasomatism, such as weathering and diagenesis. Altered plagioclase separates were obtained from 41 whole rock samples. The removed, altered plagioclase material is hereafter referred to as 'separated samples'. This material was finely ground with an agate mortar and pestle for X-ray diffraction analysis. Whole rock samples were crushed in a jawcrusher to approximately pebble sized grains then milled in a TEMA ring and puck-type grinder with a tungsten–carbide inner container to $< 200$ mesh.

#### *1.2.2. Mineralogy*

Mineralogy of separated samples was determined on a Rigaku DMAX-I X-ray diffractometer with Ni-filtered CuK$\alpha$ ($= 1.5418$ Å) radiation and JADE

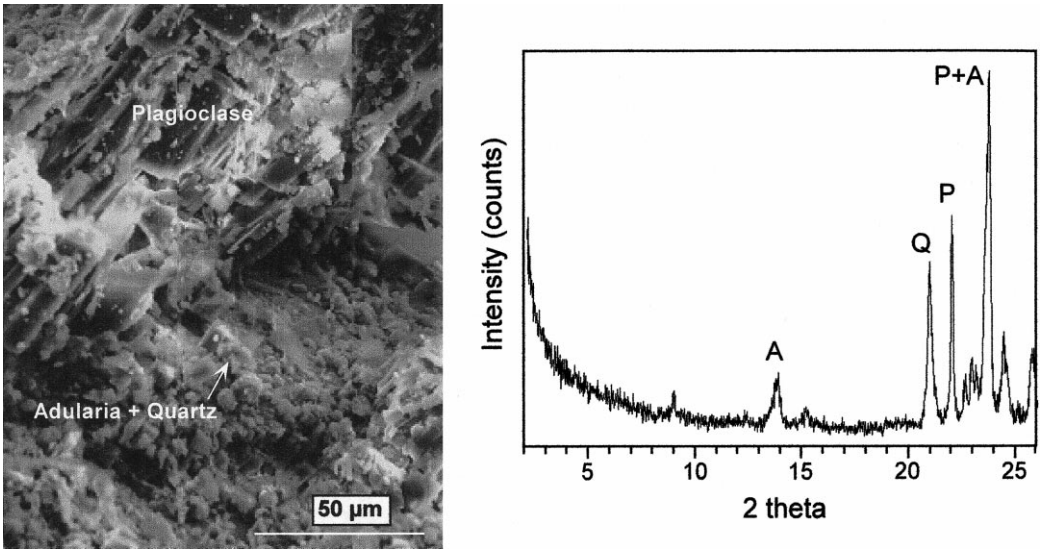


Fig. 2. SEM photo of partially dissolved plagioclase with adularia and quartz. XRD pattern shows the same assemblage; plagioclase (P) at $\sim 21.9^\circ$ $2\theta$, adularia (A) at $\sim 13.8^\circ$ and $\sim 15.1^\circ$ $2\theta$, and quartz (Q) at $\sim 20.8^\circ$ $2\theta$. Overlap of plagioclase and adularia at $\sim 23.5^\circ$ $2\theta$.

pattern-processing software. The receiving and scattering slits of the Rigaku XRD are, respectively, 1/2° and 4°. An initial 2θ angle of 2° and a final angle of 70° was used with a goniometer step size of 0.05° 2θ and count time of 1 s per step. Operating conditions were set to an accelerating voltage of 40 kV and a sample current of 25 mA. For XRD analysis, altered plagioclase was placed in an aluminum sample holder.

XRD analysis was used to estimate the relative proportions of mineral phases in separated samples, particularly adularia abundance. For each sample examined, the same volume of separated plagioclase material was used, thus allowing for comparison of the peak areas measured by JADE pattern-processing software. If plagioclase is absent in the separated sample, the amount of adularia is estimated based on the area of the peak at ~23.5° 2θ. For samples in which plagioclase is present in the assemblage, an average area factor for adularia is first calculated. The average area factor is calculated by averaging the ratios of the areas under the ~23.5° peak (adularia ± plagioclase) and the ~22.5° peak (adularia only) for each separated sample XRD scan that does not contain plagioclase within the sample set. An average area factor of 4.48 was calculated for this study. For samples in which plagioclase is present, the area of the ~22.5° adularia peak is then multiplied by the average area factor, resulting in an estimated relative abundance of adularia present in the sample. The separated samples were ranked for adularia content based on the calculated or measured area of adularia. Although this method is only semi-quantitative, it appears to provide a reasonable first approximation to the relative proportions of phases present within the separated samples.

Where applicable, semi-quantitative clay mineral analysis was performed on separated samples using three scans for each sample: air-dried, saturated with ethylene glycol, and heated at 375°C for 30 min. The method utilized for semi-quantitative clay mineral analysis allows for the determination of clay minerals to parts in ten of the clay fraction (G. Austin, personal communication, 1992; Austin and Leininger, 1976).

Morphology of the alteration products was examined using scanning electron microscopy (SEM) analysis of six carbon-coated sample chips. The SEM used was a Hitachi S450 equipped with an energy dispersive spectrometer (EDS).

### *1.2.3. Geochemistry*

Two carbon-coated polished thin sections were examined using a JEOL 733 electron microprobe

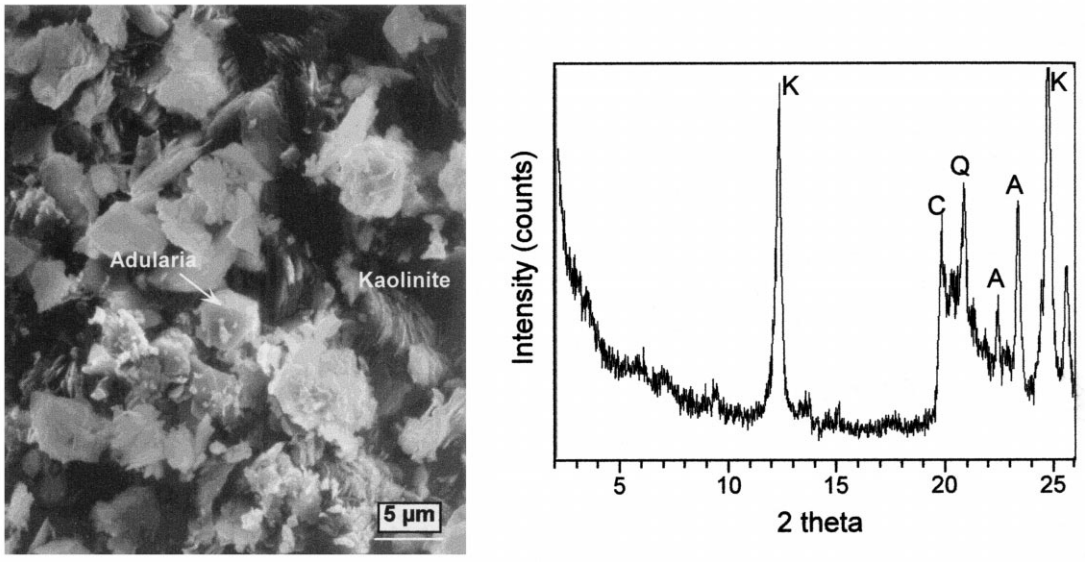


Fig. 3. SEM photo of adularia and kaolinite books. XRD pattern shows kaolinite at characteristic 2θ angle of 12.4°; K = kaolinite, C = clay 021 band, Q = quartz, A = adularia.

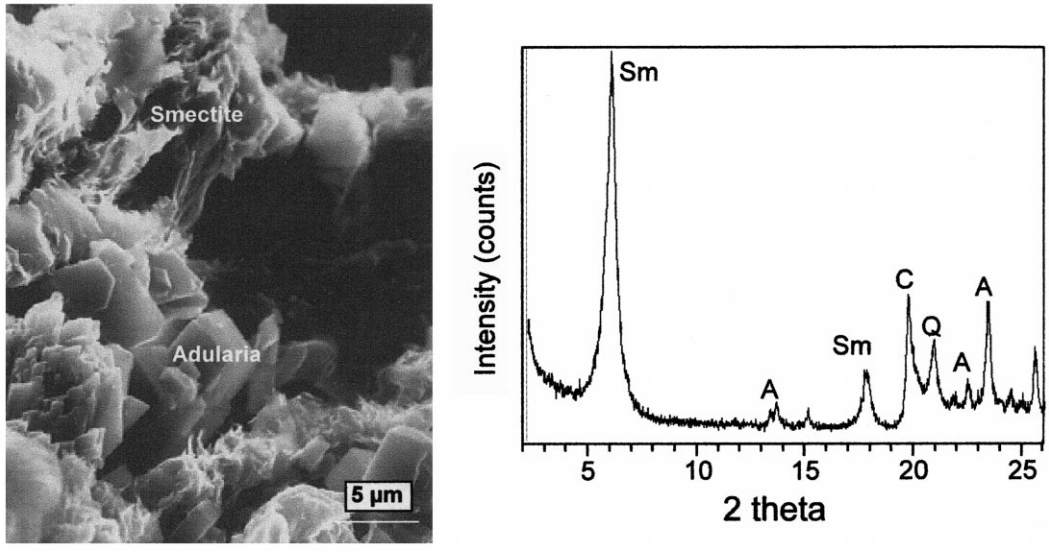


Fig. 4. SEM photo of mixed-layer I/S and euhedral adularia. XRD pattern shows the same assemblage; Mx = mixed-layer I/S, A = adularia, C = general clay peak, Q = quartz.

(EMP) equipped with five wavelength dispersive spectrometers (WDS), one EDS, and a back-scattered electron detector at the University of New Mexico. Operating conditions for the EMP during analyses were an accelerating voltage of 15 kV, a beam diameter of 1–10 μm, a beam current of 20 nA and a count time of approximately 45 s. Element distribution maps were also obtained.

X-ray fluorescence (XRF) analysis was performed following the procedure of Norrish and Chappell (1977) using a Rigaku 3062 instrument at both the New Mexico Institute of Mining and Technology

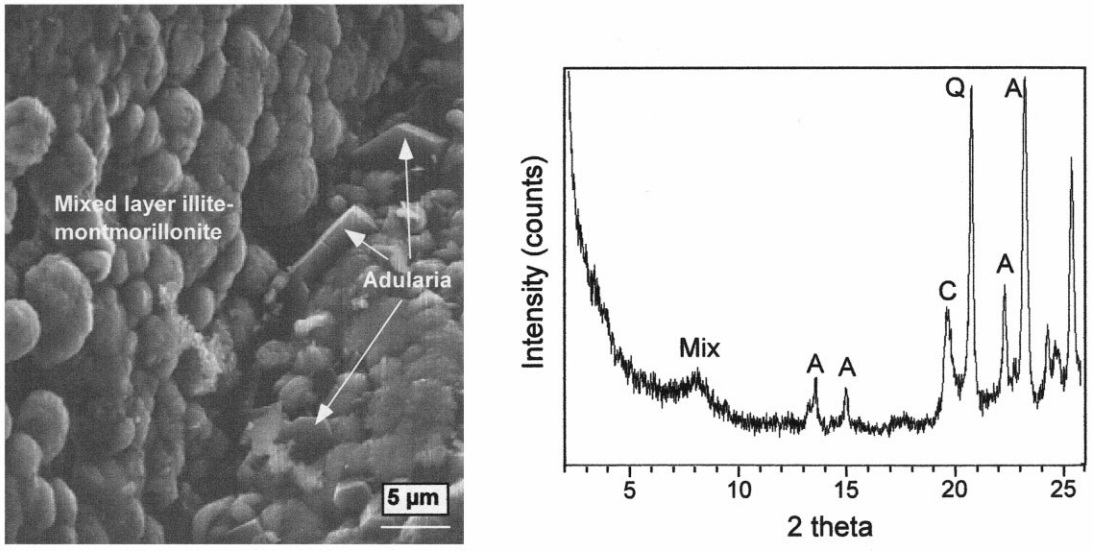


Fig. 5. SEM photo of euhedral adularia and smectite. XRD pattern shows a distinctive smectite peak at approximately 6.0° 2$\theta$; Sm = smectite, C = smectite 021 band, Q = quartz, A = adularia.

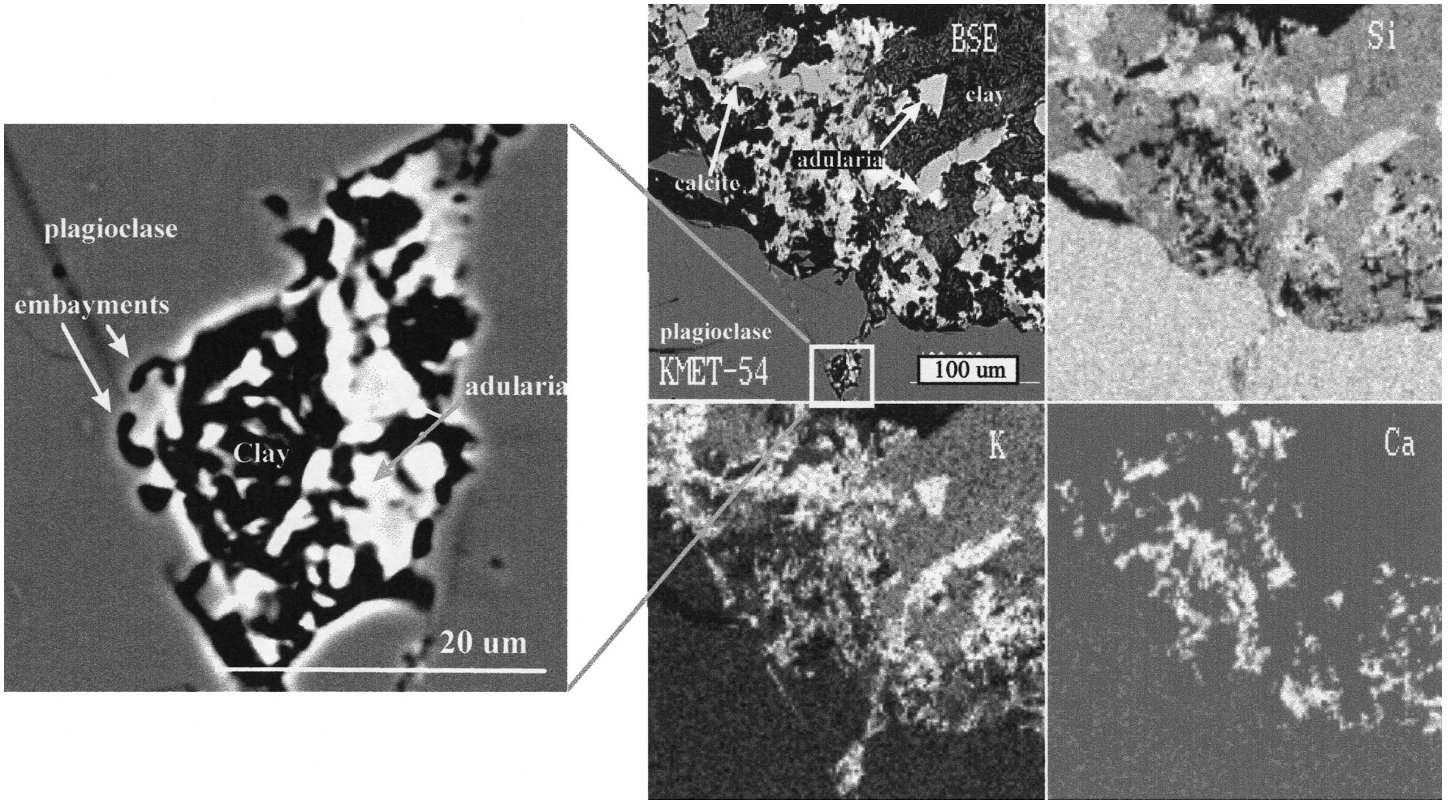


Fig. 6. Electron microprobe back-scattered image for adularia + mixed-layer I/S with element maps for silica, potassium, and calcium (higher brightness indicates greater concentrations). Plucked areas are due to sample preparation. Image at left is an enlargement of the plagioclase embayment. Note small dissolution textures within the main embayment as well as the presence of clay in direct association with plagioclase.

X-ray Fluorescence Facility and the University of New Mexico. XRF was used to analyze major elements, along with trace elements Rb, Sr, Y, Zr, Nb, Pb, Th, and U. Operating conditions were 40 kV and 25 mA at both locations, and data reduction was accomplished following the method of Norrish and Chappell (1977). Incident X-rays were generated using a rhodium end-window tube. Samples were fused into disks for major element analysis using a lithium tetraborate flux, and were prepared as pressed pellets for trace element analysis. Instrumental neutron activation analysis (INAA) of whole rock samples was performed at X-ray Assay Laboratories. INAA was performed on separated samples at New Mexico Institute of Mining and Technology after having undergone irradiation at the University of Missouri Research Reactor. Irradiation took place for approximately 40 h at a flux of $2.5 \times 10^{13}$ $N \cdot cm^{-2} \cdot s^{-1}$. Analytical errors, based on replicate analysis of samples, are as follows for major elements (in wt.%): $SiO_2 \pm 0.16$ wt.%, $TiO_2 \pm 0.01$ wt.%, $Al_2O_3 \pm 0.03$ wt.%, $Fe_2O_3 \pm 0.01$ wt.%, MnO $\pm$ 0.04

Table 2
Unaltered upper Lemitar and Hells Mesa geochemistry
nr = Not reported, oxides in wt.%, elements in ppm.

| Hells Mesa Tuff samples | | | | | | Upper Lemitar Tuff samples | | | | | | | |
|---|---|---|---|---|---|---|---|---|---|---|---|---|---|
| Sample | H.M. Tuff | 78-7-75 | 84-10-28 | 19-D | LJ4 | Lemitar | 78-6-48 | 78-6-61 | 78-6-62 | 78-6-63 | 84-5-4 | 540B | TS-23 |
| $SiO_2$ | 75.46 | 69.50 | 73.90 | 69.84 | 69.34 | 71.34 | 65.98 | 69.07 | 67.60 | 68.67 | 73.60 | 65.3 | 71.2 |
| $TiO^2$ | 0.21 | 0.33 | 0.25 | 0.37 | 0.22 | 0.50 | 0.49 | 0.40 | 0.56 | 0.42 | 0.27 | 0.65 | 0.05 |
| $Al_2O_3$ | nr | 14.83 | 13.50 | 15.12 | 14.75 | nr | 16.23 | 15.55 | 16.36 | 15.38 | 14.08 | 16.2 | 14.2 |
| $Fe_2O_3$ | 1.44 | 1.56 | 1.52 | 2.26 | 2.45 | 2.52 | 1.93 | 1.74 | 2.40 | 1.95 | 1.42 | 3.14 | 2.55 |
| MnO | 0.03 | 0.06 | 0.05 | 0.04 | 0.03 | 0.05 | 0.03 | 0.07 | 0.07 | 0.06 | 0.02 | 0.12 | 0.07 |
| MgO | 0.44 | 0.33 | 0.43 | 0.72 | 0.65 | 0.06 | 0.37 | 0.40 | 0.53 | 0.55 | 0.11 | 0.76 | 0.54 |
| CaO | nr | 0.83 | 0.90 | 1.84 | 1.63 | nr | 1.17 | 1.09 | 1.66 | 1.31 | 0.55 | 1.88 | 1.62 |
| $Na_2O$ | 3.47 | 4.24 | 3.73 | 3.90 | 3.82 | 3.93 | 4.25 | 4.51 | 4.75 | 4.30 | 3.58 | 4.33 | 4.2 |
| $K_2O$ | 4.76 | 5.54 | 4.56 | 4.47 | 4.40 | 4.80 | 5.58 | 5.58 | 5.38 | 5.11 | 5.54 | 5.05 | 4.62 |
| Zn | 24 | nr | 30.7 | nr | nr | 75 | nr | nr | nr | nr | nr | | |
| As | 2 | nr | 1.4 | nr | nr | 1 | nr | nr | nr | nr | nr | | |
| Rb | 195 | 169 | 193 | 144 | 169 | 157 | 124 | 74 | 77 | 93 | nr | 206 | 159 |
| Sr | 180 | 178 | 235 | 384 | 249 | 248 | 247 | nr | nr | nr | nr | 361 | 239 |
| Y | 18 | 71 | 11 | 27 | 34 | 80 | 41 | 78 | 60 | 80 | nr | 76 | 71 |
| Zr | 137 | 286 | 142 | 219 | 219 | 363 | 350 | 352 | 483 | 325 | nr | | |
| Nb | 23 | 30 | 23 | 26 | nr | 27 | 18 | 29 | 14 | 29 | nr | 24 | 27 |
| Ba | 524 | nr | 593 | 1028 | 1063 | 1245 | nr | nr | nr | 1299 | nr | 2290 | 1430 |
| Pb | 18 | nr | 5 | nr | nr | 31 | nr | nr | nr | nr | nr | 14 | 14 |
| Th | 39.6 | 20 | 24 | 18 | 16.80 | 22 | 14 | 50 | 14 | nr | nr | 15 | 17 |
| U | 4 | 6 | 4 | 3 | 3.6 | 4 | 9 | 20 | 6 | 0 | nr | 4.9 | 4.3 |
| Co | nr | nr | 41.0 | nr | 3.80 | nr | nr | nr | nr | nr | nr | | |
| Br | 0.3 | nr | 1 | nr | nr | 0 | nr | nr | nr | nr | nr | | |
| Sb | 0.30 | nr | 0.40 | nr | 0.50 | 0.1 | nr | nr | nr | nr | nr | | |
| Cs | 4.0 | nr | 3.0 | nr | 2.00 | 1.8 | nr | nr | nr | nr | nr | | |
| La | 42.4 | nr | 38.1 | nr | 42.60 | 70.2 | nr | nr | nr | nr | nr | 130 | 71 |
| Ce | 71 | nr | 76 | nr | 67 | 136 | nr | nr | nr | nr | nr | 210 | 150 |
| Nd | 25 | nr | 18 | nr | 36.00 | 61 | nr | nr | nr | nr | nr | 107 | 69.5 |
| Sm | 3.0 | nr | 2.7 | nr | 5.00 | 12.4 | nr | nr | nr | nr | nr | 15.7 | 12.7 |
| Eu | 0.55 | nr | 0.6 | nr | 1.22 | 1.9 | nr | nr | nr | nr | nr | 2.98 | 1.93 |
| Tb | 0.32 | nr | 0.30 | nr | 0.52 | 1.9 | nr | nr | nr | nr | nr | 1.9 | 1.8 |
| Yb | 2.0 | nr | 1.6 | nr | 2.24 | 7.0 | nr | nr | nr | nr | nr | 7.7 | 7.5 |
| Lu | 0.36 | nr | 0.26 | nr | 0.38 | 0.97 | nr | nr | nr | nr | nr | 1.13 | 1.02 |
| Hf | 4.7 | nr | 4.6 | nr | 5.50 | 10.9 | nr | nr | nr | nr | nr | 14 | 11 |
| Ta | 2.2 | nr | 2.0 | nr | 1.30 | 2.2 | nr | nr | nr | nr | nr | 1 | 2 |
| W | nr | nr | 340 | nr | nr | nr | nr | nr | nr | nr | nr | 120 | 220 |

Table 3
Upper Lemitar whole rock geochemistry
Oxides reported in wt.%, elements reported in ppm.

| Sample | KM-31 | KM-36 | KM-41 | KM-46 | KM-51 | KM-55 | KM-56 | KM-86 | KM-90 | KM-91 | KM-92 | KM-93 | KM-94 | KM-95 | KM-106 | KM-107 | KM-108 | KM-109 | KM-110 | KM-111 | KM-122 |
|---|---|---|---|---|---|---|---|---|---|---|---|---|---|---|---|---|---|---|---|---|---|
| $SiO_2$ | 77.38 | 74.79 | 67.25 | 70.60 | 62.48 | 65.77 | 66.03 | 67.49 | 71.21 | 68.67 | 65.15 | 68.26 | 66.43 | 66.18 | 64.97 | 69.18 | 71.36 | 67.11 | 66.86 | 68.91 | 68.47 |
| $TiO_2$ | 0.19 | 0.20 | 0.57 | 0.43 | 0.63 | 0.56 | 0.56 | 0.58 | 0.33 | 0.54 | 0.63 | 0.56 | 0.59 | 0.60 | 0.51 | 0.50 | 0.42 | 0.52 | 0.41 | 0.36 | 0.49 |
| $Al_2O_3$ | 11.81 | 13.04 | 15.47 | 13.37 | 17.36 | 15.99 | 15.68 | 15.43 | 14.67 | 14.94 | 16.26 | 14.84 | 15.35 | 16.05 | 15.52 | 14.59 | 13.10 | 15.60 | 15.01 | 15.01 | 15.79 |
| $Fe_2O_3$ | 1.13 | 1.69 | 2.94 | 2.04 | 3.11 | 3.23 | 2.90 | 2.83 | 1.51 | 2.81 | 2.20 | 2.86 | 2.88 | 2.98 | 2.19 | 2.41 | 2.14 | 2.54 | 1.80 | 2.44 | 2.32 |
| MnO | 0.05 | 0.06 | 0.04 | 0.04 | 0.03 | 0.07 | 0.10 | 0.06 | 0.03 | 0.03 | 0.02 | 0.04 | 0.04 | 0.02 | 0.05 | 0.04 | 0.07 | 0.04 | 0.05 | 0.05 | 0.04 |
| MgO | 0.17 | 0.34 | 0.40 | 0.55 | 1.07 | 0.42 | 0.48 | 0.39 | 0.12 | 0.30 | 0.42 | 0.22 | 0.33 | 0.30 | 0.85 | 0.39 | 0.37 | 0.42 | 0.69 | 0.41 | 0.22 |
| CaO | 0.17 | 0.31 | 0.42 | 1.32 | 0.83 | 0.40 | 0.37 | 0.48 | 0.27 | 0.44 | 0.37 | 0.44 | 0.43 | 0.43 | 1.77 | 0.51 | 0.74 | 0.34 | 1.30 | 1.20 | 0.27 |
| $Na_2O$ | 1.59 | 1.48 | 1.87 | 2.95 | 2.34 | 1.85 | 1.86 | 2.14 | 2.65 | 2.25 | 1.26 | 1.59 | 1.83 | 2.41 | 4.66 | 2.29 | 1.92 | 2.17 | 3.99 | 3.01 | 2.24 |
| $K_2O$ | 7.81 | 8.32 | 10.00 | 6.64 | 9.50 | 10.93 | 10.87 | 9.06 | 8.50 | 9.20 | 12.21 | 10.35 | 10.29 | 10.02 | 3.58 | 9.15 | 8.57 | 10.13 | 4.73 | 6.82 | 9.57 |
| Cr | 171 | 62 | 685 | 39 | 41 | 387 | 85 | 9 | 12 | 21 | 14 | 21 | 19 | 9 | 15 | 10 | 17 | 10 | 31 | 12 | 101 |
| Zn | 40 | 55 | 29 | 32 | 81 | 74 | 84 | 56 | 25 | 34 | 36 | 38 | 43 | 31 | 54 | 53 | 35 | 52 | 18 | 40 | 32 |
| As | 49 | 22 | 3 | 3 | 5 | 77 | 91 | 9 | 34 | 9 | 7 | 21 | 34 | 15 | 3 | 3 | 22 | 16 | 5 | 3 | 26 |
| Rb | 318 | 296 | 401 | 255 | 384 | 376 | 376 | 394 | 329 | 438 | 535 | 486 | 456 | 455 | 526 | 402 | 395 | 422 | 241 | 305 | 379 |
| Sr | 105 | 111 | 68 | 146 | 142 | 93 | 91 | 144 | 55 | 151 | 83 | 127 | 132 | 159 | 391 | 90 | 77 | 89 | 67 | 234 | 128 |
| Y | 18 | 14 | 17 | 58 | 69 | 73 | 70 | 75 | 75 | 65 | 67 | 61 | 68 | 66 | 59 | 68 | 62 | 69 | 144 | 26 | 59 |
| Zr | 175 | 149 | 122 | 377 | 550 | 454 | 444 | 464 | 304 | 426 | 514 | 443 | 459 | 489 | 455 | 419 | 337 | 429 | 401 | 197 | 397 |
| Ba | 478 | 2348 | 435 | 1288 | 1582 | 1493 | 1474 | 2678 | 595 | 1786 | 2186 | 1845 | 2584 | 1991 | 2247 | 1462 | 1110 | 1564 | 1319 | 967 | 2298 |
| Pb | 17 | 33 | 21 | 19 | 23 | 66 | 64 | 21 | 21 | 20 | 12 | 18 | 18 | 22 | 20 | 19 | 13 | 26 | 15 | 15 | 26 |
| Sb | 5.2 | 0.9 | 0.3 | 0.2 | 0.2 | 12.0 | 8.4 | 0.4 | 1.9 | 16.0 | 2.1 | 5.4 | 1.7 | 10.0 | 1.1 | 0.2 | < .2 | < .2 | 1.10 | < .2 | 10.0 |
| Cs | 3.2 | 5.9 | 5.0 | 4.8 | 9.5 | 3.0 | 3.5 | 6.0 | 3.0 | 8.0 | 5.0 | 4.0 | 5.0 | 4.0 | 88.0 | 5.0 | 3.0 | 2.0 | 77.0 | 8.0 | 6.0 |
| La | 34.7 | 69.3 | 38.3 | 54.9 | 82.2 | 69.2 | 67.8 | 82.8 | 86.7 | 74.8 | 78.6 | 77.2 | 69.4 | 74.6 | 90.2 | 68.2 | 60.3 | 77.2 | 114.0 | 50.1 | 122.0 |
| Ce | 78 | 140 | 52 | 121 | 165 | 151 | 141 | 148 | 158 | 134 | 146 | 137 | 126 | 138 | 153 | 128 | 112 | 142 | 201 | 83 | 209 |
| Nd | 32.2 | 57.1 | 19 | 52.9 | 69.4 | 61.7 | 59.9 | 67 | 69 | 57 | 59 | 63 | 54 | 54 | 61 | 50 | 48 | 62 | 78 | 28 | 80 |
| Sm | 8.4 | 12.0 | 2.7 | 10.3 | 13.5 | 12.9 | 12.4 | 11.7 | 12.7 | 10.4 | 10.3 | 10.2 | 9.7 | 10.0 | 10.0 | 9.6 | 9.1 | 10.6 | 12.9 | 4.4 | 13.7 |
| Eu | 0.5 | 2.3 | 0.5 | 1.6 | 2.5 | 2.3 | 2.2 | 2.1 | 1.5 | 2.4 | 2.4 | 1.9 | 2.6 | 1.9 | 1.6 | 2.0 | 1.7 | 2.1 | 1.9 | 1.2 | 2.7 |
| Yb | 5.5 | 5.6 | 2.1 | 5.7 | 6.4 | 6.8 | 6.5 | 5.7 | 5.6 | 5.0 | 4.9 | 4.7 | 5.3 | 4.8 | 4.2 | 5.0 | 5.7 | 5.7 | 5.3 | 2.7 | 5.1 |
| Lu | 0.8 | 0.7 | 0.4 | 0.8 | 0.9 | 0.9 | 0.9 | 0.9 | 0.8 | 0.8 | 0.8 | 0.7 | 0.76 | 0.76 | 0.63 | 0.80 | 0.84 | 0.83 | 0.79 | 0.41 | 0.78 |

| KM-123 | KM-124 | KM-125 | KM-126 | KM-127 | KM-128 | KM-129 | KM-130 | KM-131 | KM-138 | KM-143 | KM-144 | KM-147 | KM-148 | KM-149 | KM-150 | KM-151 | KM-154 | KM-156 | KM-157 | KM-159 | KM-16 |
|---|---|---|---|---|---|---|---|---|---|---|---|---|---|---|---|---|---|---|---|---|---|
| 74.67 | 68.13 | 71.34 | 66.86 | 65.96 | 68.66 | 72.57 | 70.04 | 72.61 | 63.83 | 64.10 | 69.06 | 72.90 | 72.05 | 71.77 | 68.47 | 69.42 | 70.07 | 68.15 | 69.80 | 69.16 | 66.57 |
| 0.26 | 0.52 | 0.33 | 0.55 | 0.62 | 0.54 | 0.42 | 0.52 | 0.43 | 0.59 | 0.51 | 0.51 | 0.39 | 0.44 | 0.43 | 0.53 | 0.50 | 0.52 | 0.55 | 0.49 | 0.54 | 0.57 |
| 12.72 | 15.89 | 14.50 | 15.59 | 15.98 | 14.93 | 13.43 | 14.70 | 12.95 | 16.79 | 17.50 | 14.53 | 13.50 | 14.00 | 14.21 | 15.29 | 14.75 | 14.21 | 15.35 | 14.61 | 14.60 | 15.43 |
| 1.50 | 2.56 | 1.71 | 2.76 | 3.18 | 2.81 | 2.21 | 2.67 | 2.32 | 3.08 | 2.36 | 2.68 | 2.05 | 2.30 | 2.26 | 2.74 | 2.69 | 2.81 | 2.98 | 2.70 | 2.85 | 3.02 |
| 0.04 | 0.04 | 0.03 | 0.05 | 0.08 | 0.06 | 0.06 | 0.07 | 0.06 | 0.08 | 0.03 | 0.05 | 0.06 | 0.05 | 0.07 | 0.03 | 0.04 | 0.02 | 0.05 | 0.06 | 0.03 | 0.07 |
| 0.07 | 0.22 | 0.11 | 0.48 | 0.37 | 0.38 | 0.32 | 0.35 | 0.36 | 0.67 | 0.30 | 0.49 | 0.41 | 0.51 | 0.39 | 0.39 | 0.40 | 0.58 | 0.38 | 0.47 | 0.29 | 0.46 |
| 0.22 | 0.39 | 0.29 | 0.60 | 0.42 | 0.61 | 0.58 | 0.85 | 0.44 | 0.57 | 0.36 | 0.40 | 0.73 | 1.11 | 0.44 | 0.49 | 0.51 | 0.30 | 0.33 | 0.48 | 0.30 | 1.19 |
| 2.42 | 2.23 | 2.94 | 2.59 | 2.24 | 2.21 | 2.89 | 3.20 | 2.27 | 2.02 | 2.85 | 1.84 | 3.28 | 3.65 | 2.73 | 2.57 | 2.72 | 1.03 | 2.11 | 2.41 | 1.53 | 1.87 |
| 7.24 | 9.38 | 8.29 | 8.87 | 10.30 | 9.21 | 7.01 | 7.26 | 7.39 | 11.43 | 10.72 | 9.97 | 5.88 | 4.79 | 7.82 | 9.22 | 8.15 | 8.90 | 9.89 | 7.33 | 10.10 | 9.26 |
| 241 | 86 | 149 | 104 | 100 | 140 | 142 | 101 | 158 | 68 | 43 | 116 | 118 | 98 | 101 | 97 | 90 | 115 | 108 | 120 | 167 | 112 |
| 33 | 48 | 24 | 53 | 47 | 46 | 42 | 51 | 43 | 54 | 46 | 44 | 47 | 49 | 38 | 44 | 41 | 40 | 45 | 57 | 59 | 67 |
| 27 | 37 | 78 | 15 | 10 | 9 | 18 | 13 | 18 | 24 | 19 | 19 | 8 | 3 | 19 | 3 | 26 | 3 | 44 | 11 | 3 | 42 |
| 285 | 367 | 319 | 364 | 453 | 384 | 278 | 282 | 313 | 504 | 402 | 378 | 226 | 168 | 309 | 136 | 320 | 386 | 490 | 342 | 452 | 397 |
| 48 | 177 | 47 | 168 | 133 | 127 | 122 | 181 | 96 | 118 | 146 | 76 | 121 | 206 | 114 | 56 | 113 | 65 | 127 | 106 | 111 | 184 |
| 72 | 64 | 75 | 78 | 66 | 71 | 79 | 70 | 67 | 70 | 76 | 59 | 84 | 74 | 83 | 117 | 79 | 57 | 71 | 68 | 63 | 70 |
| 235 | 450 | 293 | 442 | 484 | 414 | 309 | 390 | 338 | 493 | 468 | 416 | 278 | 327 | 330 | 418 | 380 | 417 | 421 | 382 | 419 | 433 |
| 633 | 2687 | 579 | 2285 | 2222 | 1718 | 989 | 1500 | 1055 | 1878 | 1981 | 1458 | 739 | 1093 | 1060 | 1458 | 1100 | 1605 | 1822 | 1278 | 2683 | 2728 |
| 18 | 23 | 26 | 21 | 23 | 20 | 18 | 17 | 18 | 24 | 25 | 17 | 17 | 19 | 20 | 60 | 25 | 13 | 25 | 22 | 25 | 18 |
| 10.0 | 8.3 | 5.9 | 1.2 | 0.4 | 130 | < .2 | 0.5 | 0.4 | 130 | < .2 | < .2 | < .2 | < .2 | 0.4 | 0.5 | < .2 | 11.0 | 1.3 | 0.5 | 2.7 | 3.0 |
| 4.0 | 4.0 | 3.0 | 5.0 | 3.0 | 4.0 | 2.0 | 3.0 | 4.0 | 2.0 | 4.0 | 3.0 | 3.0 | 1.0 | 3.0 | 3.0 | 2.0 | 8.0 | 3.0 | 6.0 | 3.0 | 7.0 |
| 70.1 | 121.0 | 93.1 | 83.2 | 69.3 | 66.2 | 59.8 | 64.7 | 61.2 | 72.9 | 105.0 | 65.2 | 57.5 | 62.1 | 66.7 | 66.9 | 60.2 | 65.8 | 70.0 | 59.8 | 62.6 | 71.2 |
| 134 | 205 | 165 | 152 | 127 | 117 | 117 | 124 | 111 | 129 | 188 | 118 | 112 | 118 | 121 | 124 | 114 | 121 | 128 | 111 | 116 | 131 |
| 58 | 79 | 70 | 58 | 53 | 55 | 51 | 49 | 48 | 57 | 70 | 52 | 49 | 51 | 51 | 51 | 47 | 49 | 55 | 50 | 50 | 52 |
| 11.5 | 13.7 | 13.4 | 11.1 | 9.7 | 10.0 | 10.1 | 9.7 | 9.0 | 10.2 | 11.8 | 9.2 | 10.1 | 9.9 | 10.5 | 9.6 | 10.0 | 8.9 | 10.1 | 8.9 | 8.6 | 9.8 |
| 0.7 | 3.0 | 1.5 | 2.8 | 2.3 | 1.8 | 1.3 | 1.6 | 1.1 | 2.3 | 2.6 | 1.5 | 1.5 | 1.3 | 1.4 | 2.4 | 1.5 | 2.1 | 1.7 | 1.4 | 1.3 | 2.1 |
| 5.7 | 5.0 | 6.2 | 6.6 | 4.8 | 5.6 | 6.2 | 5.7 | 5.2 | 5.1 | 4.8 | 4.5 | 6.8 | 5.7 | 6.4 | 5.5 | 6.2 | 4.2 | 5.6 | 5.2 | 4.8 | 5.4 |
| 0.79 | 0.72 | 0.93 | 0.95 | 0.73 | 0.82 | 0.94 | 0.83 | 0.75 | 0.73 | 0.74 | 0.73 | 1.03 | 0.87 | 0.94 | 0.81 | 0.89 | 0.67 | 0.84 | 0.81 | 0.71 | 0.81 |

wt.%, MgO ± 0.04 wt.%, CaO ± 0.11 wt.%; $Na_2O$ ± 0.04 wt.%, $K_2O$ ± 0.03 wt.%, $P_2O_5$ ± 0.01 wt.%, and for trace elements (in ppm) V ± 4, Cr ± 12, Ni ± 1, Cu ± 1, Zn ± 1, Ga ± 0.3, As ± 0.7, Rb ± 0.8, Sr ± 0.7, Y ± 1, Zr ± 8, Nb ± 0.1, Mo ± 0.1, Ba ± 10, Pb ± 0.2, Th ± 1, U ± 0.5, Sc ± 0.04, Co ± 0.13, Br ± 0.07, Sb ± 0.1, Cs ± 1.4, La ± 1.8, Ce ± 1.4, La ± 1.8, Ce ± 1.4, Nd ± 0.7, Sm ± 0.07, Eu ± 0.14, Tb ± 0.02, Yb ± 0.07, Lu ± 0.01, Hf ± 0.12, Ta ± 0.04, W ± 0.05.

## 2. Results

### *2.1. Mineralogy*

#### *2.1.1. Mineral abundances, morphology and element mapping*

Unmetasomatized upper Lemitar and Hells Mesa Tuff samples examined in thin section show no significant signs of plagioclase alteration, however, one fresh Hells Mesa Tuff sample does show a minor amount of plagioclase replacement by clay or possibly calcite. The unaltered nature of plagioclase in fresh upper Lemitar and Hells Mesa Tuff samples outside of the K-metasomatism area indicates the mineralogy found in the separated samples is attributable to an alteration process other than weathering. The mineral assemblage of the separated samples consists of variable combinations of adularia, quartz, kaolinite, mixed-layer illite–smectite (I/S), discrete smectite, discrete illite, and remnant plagioclase with minor calcite and barite.

Adularia, a low-temperature K-feldspar, is present in all 41 of the separated samples (Table 1) and consistently displays euhedral habit. Fine-grained quartz is also present in all 41 separated samples and tends to display an amorphous, globular habit. Residual plagioclase was found in 17 of the 41 separated samples and consistently appears partially dissolved in SEM images (Table 1; Fig. 2) suggesting chemical instability during the conditions imposed during potassic alteration.

The most common clay types found in the alteration mineral assemblage are kaolinite and mixed-layer I/S with each being present in 19 of the separated samples. Kaolinite is typically a major clay constituent, 16 of the 19 samples have ≥ 5 parts per 10 kaolinite in the clay fraction, and is found spatially associated with adularia (Fig. 3). Mixed-layer I/S is also a major clay component and is found in quantities ≥ 5 parts per 10 in 11 of the 19 separated samples. When present, mixed-layer I/S appears to be either metastable or near equilibrium with adularia, for both minerals show no apparent indication of dissolution when in the same assemblage (Fig. 4).

In contrast to the frequent occurrence of kaolinite and mixed-layer I/S, significant abundances of discrete smectite and discrete illite are uncommon in the alteration assemblage. Large quantities, ≥ 5 parts per 10 of the clay fraction, of discrete smectite are present in only two of the 41 separated samples with trace quantities found in 12 samples. Smectite tends to be subhedral and typically coats euhedral adularia crystals (Fig. 5). Discrete illite is also scarce with only three samples containing ≥ 5 parts per 10 illite and trace amounts in nine of the 41 samples.

Calcite is present in at least four of the separated samples from the Socorro K-metasomatized area, which has not been documented previously. When present, calcite is extremely fine-grained and found in exceedingly small amounts. Barite is also found within a few samples collected in the vicinity of the Luis Lopez manganese district.

The back-scattered electron microprobe image of a polished thin section (sample KM-48) from the Hells Mesa Tuff shows a sharp boundary between the minerals in the alteration assemblage and residual plagioclase (Fig. 6). An enlargement of the plagioclase embayment shows additional, smaller embayments at the margin between plagioclase and the alteration phases (Fig. 6 inset). The dominant K-rich phase in the alteration assemblage appears to be adularia while the clay matrix is somewhat K-rich, suggesting mixed-layer I/S. This is supported by semi-quantitative clay analysis which resolved mixed-layer I/S to be the dominant clay mineral present in this sample. The Ca-map indicates the presence of extremely fine-grained calcite within the alteration assemblage.

### *2.2. Geochemistry*

#### *2.2.1. Upper Lemitar and Hells Mesa Tuffs*

*2.2.1.1. Whole rock major element concentrations.* Despite overall similarity between the upper Lemitar and Hells Mesa Tuffs, there are distinct chemical

Table 4
Hells Mesa whole rock geochemistry
Oxides reported in wt.%, elements reported in ppm.

| Sample | KM-54 | KM-58 | KM-59 | KM-60 | KM-61 | KM-96 | KM-102 | KM-112 | KM-113 | KM-114 | KM-115 | KM-116 | KM-117 | KM-118 | KM-119 | KM-120 | KM-121 | KM-153 | KM-155 | KM-158 |
|---|---|---|---|---|---|---|---|---|---|---|---|---|---|---|---|---|---|---|---|---|
| $SiO_2$ | 72.79 | 72.80 | 74.96 | 72.36 | 75.90 | 74.52 | 73.03 | 73.38 | 71.18 | 71.81 | 73.33 | 73.51 | 71.65 | 73.95 | 74.11 | 73.47 | 74.37 | 77.27 | 78.47 | 75.54 |
| $TiO_2$ | 0.27 | 0.30 | 0.24 | 0.26 | 0.22 | 0.24 | 0.25 | 0.26 | 0.29 | 0.28 | 0.23 | 0.24 | 0.41 | 0.22 | 0.22 | 0.25 | 0.21 | 0.16 | 0.15 | 0.21 |
| $Al_2O_3$ | 13.26 | 14.47 | 14.03 | 13.53 | 13.30 | 12.92 | 13.34 | 13.25 | 14.11 | 13.77 | 13.13 | 13.07 | 13.41 | 12.91 | 13.00 | 13.78 | 12.87 | 11.33 | 11.88 | 13.00 |
| $Fe_2O_3$ | 2.22 | 2.18 | 1.77 | 1.98 | 1.85 | 1.61 | 1.62 | 1.99 | 2.11 | 2.01 | 1.55 | 1.85 | 2.81 | 1.65 | 1.65 | 1.77 | 1.59 | 1.09 | 1.13 | 1.50 |
| MnO | 0.08 | 0.02 | 0.02 | 0.09 | 0.06 | 0.01 | 0.01 | 0.05 | 0.05 | 0.04 | 0.05 | 0.05 | 0.04 | 0.07 | 0.04 | 0.04 | 0.03 | 0.03 | 0.01 | 0.03 |
| MgO | 0.37 | 0.64 | 0.41 | 0.48 | 0.35 | 0.23 | 0.21 | 0.33 | 0.29 | 0.28 | 0.27 | 0.25 | 0.45 | 0.44 | 0.30 | 0.23 | 0.30 | 0.08 | 0.34 | 0.39 |
| CaO | 0.79 | 0.36 | 0.28 | 1.79 | 0.61 | 0.17 | 0.22 | 0.27 | 0.46 | 0.43 | 0.20 | 0.44 | 0.86 | 0.69 | 0.50 | 0.90 | 0.64 | 0.10 | 0.04 | 0.53 |
| $Na_2O$ | 1.42 | 0.99 | 1.26 | 1.67 | 2.53 | 0.60 | 0.71 | 1.12 | 1.63 | 1.16 | 0.80 | 2.00 | 2.29 | 2.85 | 2.18 | 3.14 | 2.66 | 0.83 | 0.11 | 2.61 |
| $K_2O$ | 7.83 | 8.39 | 7.27 | 7.18 | 6.28 | 8.52 | 8.86 | 7.60 | 7.69 | 8.79 | 8.49 | 6.79 | 6.23 | 5.82 | 6.37 | 5.70 | 5.62 | 8.74 | 5.83 | 5.10 |
| $P_2O_5$ | 0.05 | 0.05 | 0.04 | 0.05 | 0.04 | 0.06 | 0.06 | 0.07 | 0.08 | 0.08 | 0.06 | 0.07 | 0.13 | 0.07 | 0.06 | 0.07 | 0.06 | 0.02 | 0.03 | 0.05 |
| LOI | 0.15 | 0.18 | 0.18 | 0.33 | 0.06 | 1.06 | 1.21 | 1.73 | 1.59 | 1.78 | 1.56 | 1.36 | 1.47 | 0.87 | 1.43 | 0.84 | 1.23 | 0.66 | 2.45 | 1.32 |
| V | na | na | na | na | na | 22 | 28 | 35 | 42 | 30 | 27 | 35 | 60 | 30 | 31 | 33 | 34 | 26 | 24 | 26 |
| Cr | 562 | 268 | 510 | 461 | 641 | 26 | 19 | 144 | 165 | 134 | 137 | 151 | 171 | 182 | 190 | 148 | 177 | 227 | 144 | 129 |
| Ni | na | na | na | na | na | < 5 | < 5 | 6.7 | 6.3 | < 5 | 5 | 5.3 | 8.2 | 5 | 9.5 | 6.4 | < 5 | 6.2 | < 5 | 5.7 |
| Cu | na | na | na | na | na | 12.6 | 10.7 | 8.8 | 8.7 | 6.1 | 10 | < 5 | 10.8 | < 5 | 5 | 6 | 7.7 | 7.3 | 10.2 | < 5 |
| Zn | 33 | 74 | 52 | 30 | 45 | 104 | 52 | 69 | 56 | 59 | 44 | 39 | 45 | 32 | 35 | 28 | 31 | 18 | 84 | 24 |
| Ga | na | na | na | na | na | 16 | 15 | 16 | 16 | 16 | 16 | 16 | 17 | 15 | 16 | 16 | 16 | 14 | 17 | 15 |
| As | 9.2 | 16.1 | 13.0 | 6.2 | 10.3 | 4 | 11.1 | 17.6 | 7.8 | 8.1 | 10.4 | 4.5 | 7.8 | 11.6 | 10.5 | 8.2 | 5.5 | 9 | 4.8 | 3 |
| Rb | 424 | 310 | 341 | 335 | 305 | 335 | 311 | 372 | 328 | 375 | 419 | 340 | 353 | 291 | 330 | 261 | 297 | 306 | 277 | 251 |
| Sr | 120 | 16 | 77 | 92 | 117 | 88 | 98 | 75 | 144 | 111 | 74 | 110 | 214 | 151 | 147 | 230 | 171 | 27 | 40 | 118 |
| Y | 60 | 61 | 20 | 21 | 17 | 22 | 25 | 21 | 28 | 26 | 28 | 22 | 27 | 18 | 22 | 21 | 20 | 64 | 18 | 19 |
| Zr | 444 | 152 | 157 | 138 | 134 | 134 | 151 | 140 | 175 | 158 | 136 | 135 | 159 | 127 | 129 | 155 | 126 | 155 | 108 | 119 |
| Nb | 23 | 28 | 31 | 26 | 29 | 23 | 23 | 22 | 22 | 22 | 25 | 23 | 19 | 24 | 23 | 24 | 24 | 28 | 22 | 24 |
| Mo | na | na | na | na | na | < 3 | < 3 | 8.3 | 9.1 | 7.4 | 7.2 | 8.7 | 8.3 | 10.5 | 9.7 | 9.1 | 10.7 | 10.7 | 8.4 | 6.9 |
| Ba | 794 | 998 | 600 | 511 | 502 | 858 | 1187 | 773 | 1622 | 1586 | 1911 | 636 | 1742 | 1044 | 2073 | 2274 | 1362 | 275 | 598 | 473 |
| Pb | 26 | 34 | 19 | 17 | 29 | 182 | 327 | 39 | 28 | 29 | 36 | 16 | 33 | 58 | 24 | 29 | 25 | 17 | 278 | 19 |
| Th | 19 | 27 | 30 | 26 | 29 | 25 | 22 | 25 | 22 | 20 | 30 | 27 | 21 | 29 | 28 | 26 | 29 | 22 | 29 | 30 |
| U | 4 | 5 | 10 | 9 | 9 | 8 | 5 | 6 | 5 | 4 | 7 | 6 | 6 | 5 | 5 | 5 | 6 | 6 | 8 | 5 |
| Sb | 0.54 | 0.55 | 3.0 | 0.48 | 0.57 | 3.2 | 1.4 | 0.9 | 0.4 | 0.5 | 0.8 | 0.7 | 1.0 | 0.7 | 0.4 | 0.5 | 1.0 | 7.0 | 1.7 | 0.3 |
| Cs | 8.3 | 20.0 | 10.5 | 10.3 | 12.3 | 4.0 | 4.0 | 21.0 | 6.0 | 8.0 | 14.0 | 9.0 | 22.0 | 11.0 | 10.0 | 5.0 | 18.0 | 3.0 | 8.0 | 4.0 |
| La | 39.5 | 41.4 | 42.7 | 39.1 | 36.7 | 45.9 | 54.4 | 42.1 | 45.3 | 45.1 | 45.6 | 45.3 | 46.6 | 43.3 | 44.0 | 49.2 | 44.7 | 32.4 | 47.0 | 41.4 |
| Ce | 69 | 77 | 76 | 67 | 66 | 69 | 74 | 71 | 89 | 75 | 70 | 71 | 73 | 65 | 65 | 76 | 69 | 62 | 69 | 59 |
| Nd | 21.4 | 26.6 | 22.2 | 19.6 | 17.4 | 21 | 23 | 20 | 24 | 24 | 20 | 19 | 20 | 17 | 16 | 23 | 19 | 26 | 20 | 15 |
| Sm | 3.3 | 4.6 | 3.4 | 3.3 | 2.6 | 2.8 | 3.2 | 3.0 | 3.9 | 3.8 | 2.9 | 2.9 | 4.3 | 2.2 | 2.5 | 3.1 | 2.5 | 5.4 | 2.8 | 1.9 |
| Eu | 0.7 | 0.8 | 0.6 | 0.7 | 0.5 | 0.6 | 0.8 | 0.8 | 0.8 | 0.7 | 0.7 | 0.5 | 1.0 | 0.6 | < .5 | 0.8 | 0.3 | 0.5 | 0.6 | 0.5 |
| Yb | 2.1 | 2.4 | 2.6 | 2.5 | 2.3 | 2.4 | 2.5 | 2.4 | 2.6 | 2.7 | 2.5 | 2.7 | 2.7 | 1.9 | 2.2 | 2.5 | 2.0 | 5.0 | 1.9 | 2.0 |
| Lu | 0.34 | 0.35 | 0.42 | 0.41 | 0.37 | 0.35 | 0.36 | 0.40 | 0.43 | 0.44 | 0.46 | 0.44 | 0.45 | 0.34 | 0.39 | 0.43 | 0.35 | 0.74 | 0.33 | 0.32 |

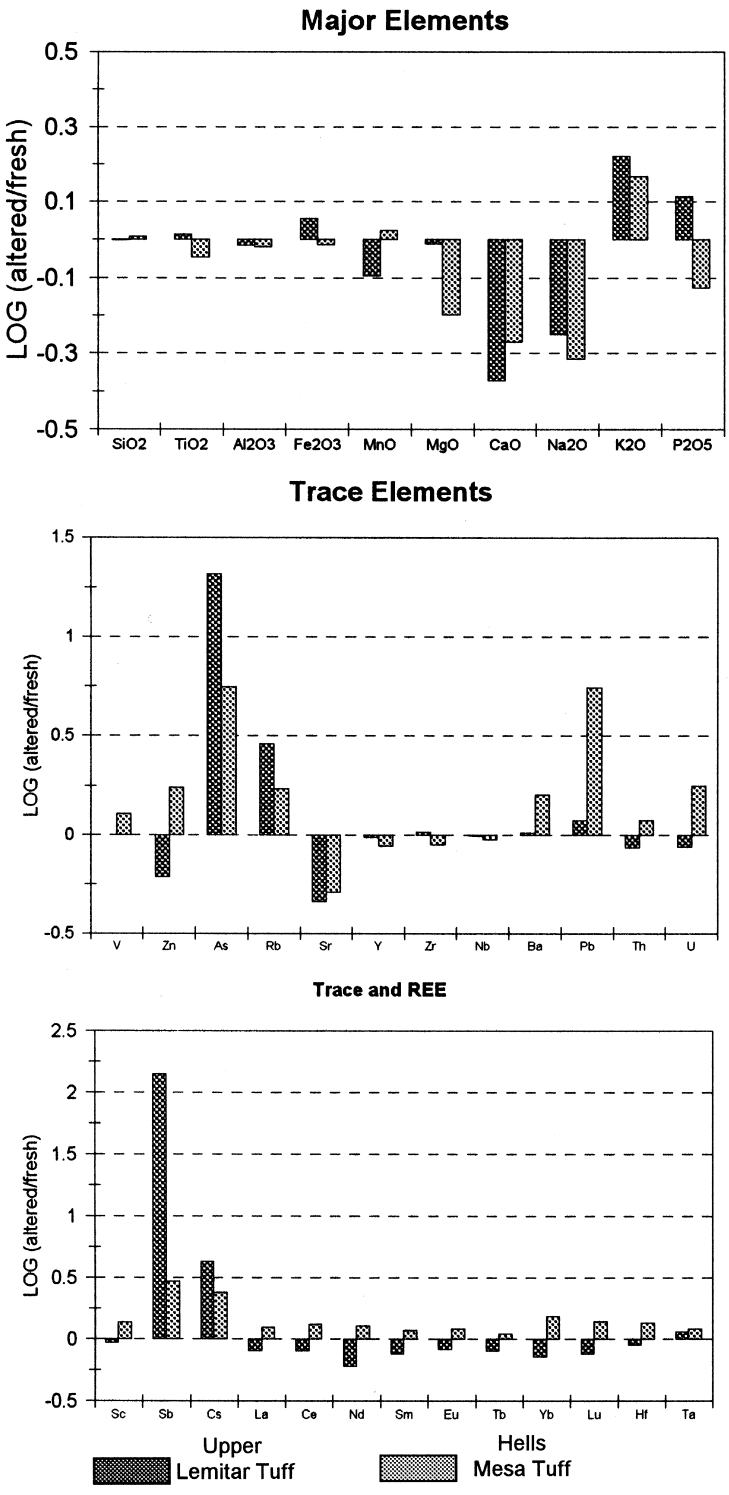
Major Elements
LOG (altered/fresh)
0.5
0.3
0.1
-0.1
-0.3
-0.5
SiO2
TiO2
Al2O3
Fe2O3
MnO
MgO
CaO
Na2O
K2O
P2O5
Trace Elements
LOG (altered/fresh)
1.5
1
0.5
0
-0.5
V
Zn
As
Rb
Sr
Y
Zr
Nb
Ba
Pb
Th
U
Trace and REE
LOG (altered/fresh)
2.5
2
1.5
1
0.5
0
-0.5
Sc
Sb
Cs
La
Ce
Nd
Sm
Eu
Tb
Yb
Lu
Hf
Ta
Upper
Lemitar Tuff
Hells
Mesa Tuff

differences between the two units. The $SiO_2$ content of fresh upper Lemitar Tuff is ~69 wt.% and that of the Hells Mesa Tuff is ~72 wt.%, with $K_2O$ and $Na_2O$ values for the two units averaging ~5 wt.% $K_2O$ and ~4 wt.% $Na_2O$ (Table 2). $K_2O/Na_2O$ ratios for unaltered samples utilized in this study are between 1.13 and 1.55, which is typical for unaltered rhyolite samples (Nockolds et al., 1978).

K-metasomatized upper Lemitar ignimbrite samples generally contain >66 wt.% $SiO_2$, 3.6–12.2 wt.% $K_2O$, and 1.0–4.7 wt.% $Na_2O$ (Table 3), while the Hells Mesa Tuff contains >71 wt.% $SiO_2$, 5.1 to 8.8 wt.% $K_2O$ and 0.6 to 3.1 wt.% $Na_2O$ (Table 4). $K_2O/Na_2O$ ratios for whole rock samples within the K-anomaly range from 0.77 to 9.69 for the upper Lemitar Tuff and 1.8–14.2 for the Hells Mesa Tuff and are characterized by both $K_2O$ enrichment and $Na_2O$ depletion (Ennis, 1996).

Enrichment/depletion diagrams comparing fresh to altered samples from the Lemitar and Hells Mesa tuff indicate a significant amount of $K_2O$, CaO, and $Na_2O$ mobility during K-metasomatism (Fig. 7). CaO content of altered samples for the two units ranges from 0.1 to 1.8 wt.%; CaO of unaltered samples are around are ~1.15 wt.% for both units. Other slightly variable major elements include MgO and $P_2O_5$ (Fig. 7). The remaining major oxides, $SiO_2$, $TiO_2$, $Al_2O_3$, $Fe_2O_3$, and MnO, show neither significant enrichment nor depletion as a result of K-metasomatism.

*2.2.1.2. Whole rock trace element concentrations*. A number of trace elements in altered upper Lemitar and Hells Mesa whole rock samples show consistent enrichment or depletion as a result of K-metasomatism. When compared to unaltered samples, metasomatized whole rock upper Lemitar and Hells Mesa Tuff samples show significant enrichment of Rb and depletion of Sr (Fig. 7) resulting in Rb/Sr ratios of 0.82 to 6.8 for the upper Lemitar Tuff and 1.1 to 19.4 for the Hells Mesa Tuff.

Other trace elements that are consistently enriched within altered samples include Ba, As, Sb and Cs (Fig. 7). Values for As within upper Lemitar Tuff whole rock samples are as high as 90.6 ppm, and Sb was found to have concentrations up to 130 ppm. Many samples containing elevated concentrations of As and Sb were collected near areas of recognized areas of hydrothermal activity, which may account for the extremely high concentration of these elements (discussed later).

Although some trace elements show consistent enrichment or depletion within K-metasomatized samples, the majority appear to be unaffected by the alteration. The trace elements V, Ga, Y, Zr, Nb, Pb, Th, Sc, Nd, Hf, and Ta show little variation on enrichment/depletion diagrams (Fig. 7), indicating that these elements are unaffected by K-metasomatism.

Most elements appear to behave similarly between the upper Lemitar and Hells Mesa Tuffs during K-metasomatism, however, several trace elements within whole rock samples of the tuff units show distinctly different trends upon K-metasomatic alteration. The elements Zn, U, La, Ce, Sm, Eu, Tb, Yb, Lu, and U all display depletion in the upper Lemitar Tuff, but enrichment in the Hells Mesa Tuff (Fig. 7). Although the magnitude of enrichment or depletion of these elements is relatively minor, the trend is striking, especially within the heavy rare earth elements (HREE). The REE Sm, Eu, and Tb display variable concentrations when compared to unaltered samples, yet show net depletion in the upper Lemitar Tuff and enrichment in the Hells Mesa Tuff whole rock samples.

*2.2.1.3. Neutron activation analysis of separated samples*. The separated samples, obtained from hand-picked relict plagioclase crystals, analyzed in this study allow the clearest and strongest picture of the chemical processes that occur during K-metasomatism because they provide a chemical signature of the alteration process that is undiluted by unaltered phases in the rock sample. Geochemical investigation of separated samples allows a detailed chemical examination of the alteration assemblage. For this study, two unaltered separated samples, one

Fig. 7. Enrichment/depletion diagrams for major and trace elements in whole rock samples. The enrichment/depletion factors are based on averages of eight unaltered upper Lemitar Tuff samples and eight unaltered Hells Mesa Tuff samples.

Table 5
Upper lemitar and hells mesa separated sample geochemistry
Oxides reported in wt.%, elements reported in ppm.

| Sample | KJH-26 | KM-31 | KM-36 | KM-41 | KM-46 | KM-51 | KM-54 | KM-55 | KM-56 | KM-58 | KM-59 | KM-60 | KM-61 | KM-86 | KM-90 | KM-91 | KM-94 | KM-95 | KM-96 | KM-102 | KM-107 | KM-111 |
|---|---|---|---|---|---|---|---|---|---|---|---|---|---|---|---|---|---|---|---|---|---|---|
| $Na_2O$ | 6.86 | 4.70 | 0.27 | 1.45 | 3.70 | 1.0 | 0.13 | 0.55 | 0.60 | 0.11 | 0.10 | 0.85 | 2.75 | 3.07 | 0.57 | 1.16 | 0.30 | 0.36 | 0.16 | 0.19 | 1.65 | 4.53 |
| FeO | 0.27 | 0.18 | 0.84 | 0.94 | 1.17 | 0.59 | 0.80 | 0.89 | 0.92 | 0.64 | 0.62 | 0.51 | 0.67 | 0.89 | 0.87 | 1.0 | 0.80 | 0.99 | 1.34 | 1.31 | 0.84 | 0.46 |
| Sc | 0.23 | 0.1 | 11.0 | 2.0 | 3.9 | 5.7 | 4.8 | 9.7 | 5.3 | 2.7 | 2.3 | 4.5 | 4.5 | 8.5 | 34.1 | 10.3 | 11.6 | 23.4 | 3.4 | 5.1 | 1.7 | 3.5 |
| Co | 0.14 | 0.11 | 3.48 | 5.25 | 6.05 | 2.17 | 8.49 | 3.33 | 2.6 | 2.2 | 1.4 | 1.7 | 2.1 | 2.0 | 3.6 | 3.5 | 3.7 | 3.2 | 3.9 | 4.3 | 71.4 | 12.2 |
| Zn | 5.9 | nr | 165 | 35.2 | 30.2 | 70.1 | 79.2 | 215 | 204 | 98.5 | 114.6 | 103.7 | 116.6 | 87 | 184 | 167 | 141 | 87 | 248 | 120 | 27 | 31 |
| As | < 0.5 | 1.24 | 5.86 | 1.49 | 3.10 | 0.82 | 6.61 | 108.0 | 69.0 | 40.1 | 32.1 | 2.95 | 8.9 | 5.55 | 108.6 | 5.0 | 11.9 | 8.0 | 3.9 | 2.2 | 1.1 | 3.9 |
| Br | 0.26 | 0.10 | 0.40 | 0.35 | 1.17 | 2.25 | 0.21 | 0.10 | 0.22 | 0.08 | 0.08 | 0.06 | 0.34 | 0.72 | 1.93 | 0.78 | 3.2 | 0.68 | 1.31 | 0.68 | 1.26 | 0.91 |
| Rb | 1 | 110 | 510 | 512 | 187 | 211 | 382 | 519 | 483 | 411 | 294 | 223 | 309 | 420 | 662 | 617 | 552 | 517 | 508 | 421 | 475 | 205.0 |
| Sr | na | na | na | na | na | na | na | na | na | na | na | na | na | 141 | nd | nd | nd | 36 | 35 | 49 | nd | 586 |
| Sb | 0.01 | 0.10 | 0.32 | 0.19 | 0.10 | 0.06 | 0.12 | 9.74 | 3.77 | 0.26 | 0.74 | 0.10 | 0.19 | 0.16 | 2.21 | 5.01 | 0.72 | 2.5 | 8.6 | 1.07 | 0.14 | 0.09 |
| Cs | 0.08 | 0.22 | 23.9 | 8.7 | 4.7 | 13.6 | 25.4 | 12.4 | 8.7 | 17.9 | 17.2 | 14.6 | 50.1 | 14.8 | 90.3 | 91.7 | 25.1 | 24.4 | 13.2 | 16.3 | 3.1 | 5.0 |
| Ba | 664 | 112 | 3600 | 289 | 1259 | 262 | 747 | 3771 | 25 051 | 257 | 4386 | 179 | 440 | 2416 | 641 | 1074 | 4526 | 861 | 651 | 1566 | 1787 | 709 |
| La | 22.3 | 3.5 | 16.1 | 12.5 | 42.2 | 11.4 | 12.9 | 70.0 | 48.8 | 15.3 | 13.5 | 69.4 | 15.1 | 27.0 | 55.1 | 31.8 | 13.98 | 17.91 | 11.51 | 24.09 | 27.18 | 27.59 |
| Ce | 32.4 | 4.9 | 44.1 | 31.8 | 76.0 | 21.9 | 32.7 | 95.7 | 93.5 | 21.3 | 24.5 | 33.0 | 65.7 | 73.6 | 140.2 | 84.8 | 32.3 | 47.7 | 22.2 | 39.3 | 77.2 | 49.6 |
| Nd | 9.7 | nd | 18 | 7.4 | 26.78 | 7.72 | 8.2 | 44.3 | 38.5 | 7.12 | 2.9 | 42.8 | 8.3 | 26.7 | 56.0 | 29.0 | 15.7 | 17.3 | 6.1 | 9.9 | 27.3 | 23.2 |
| Sm | 1.15 | 0.23 | 3.9 | 1.6 | 4.3 | 1.5 | 2.0 | 6.2 | 8.7 | 1.21 | 1.13 | 6.8 | 1.72 | 5.9 | 13.8 | 5.9 | 3.2 | 4.0 | 1.2 | 2.3 | 6.7 | 4.4 |
| Eu | 1.73 | 0.74 | 0.80 | 0.34 | 1.11 | 0.44 | 0.65 | 1.00 | 1.4 | 0.27 | 0.29 | 1.5 | 0.69 | 1.39 | 1.40 | 1.3 | 0.66 | 0.84 | 0.24 | 0.45 | 1.87 | 1.32 |
| Tb | 0.11 | 0.05 | 0.55 | 0.23 | 0.48 | 0.23 | 0.32 | 0.76 | 1.5 | 0.15 | 0.25 | 0.81 | 0.26 | 0.88 | 2.38 | 0.71 | 0.49 | 0.57 | 0.29 | 0.33 | 1.02 | 0.53 |
| Yb | 0.45 | 0.33 | 1.34 | 0.95 | 1.86 | 1.35 | 1.40 | 2.50 | 5.6 | 0.78 | 1.6 | 4.2 | 1.3 | 2.23 | 5.15 | 1.4 | 1.48 | 1.52 | 1.41 | 1.2 | 2.5 | 1.65 |
| Lu | 0.08 | 0.04 | 0.16 | 0.15 | 0.28 | 0.22 | 0.20 | 0.37 | 0.80 | 0.10 | 0.26 | 0.64 | 2.0 | 0.31 | 0.62 | 0.18 | 0.19 | 0.20 | 0.21 | 0.17 | 0.51 | 0.24 |
| Hf | 1.31 | 0.57 | 1.75 | 2.09 | 4.05 | 5.27 | 2.85 | 4.47 | 5.6 | 3.0 | 2.6 | 1.4 | 2.5 | 2.71 | 3.4 | 2.1 | 2.6 | 2.5 | 1.5 | 1.8 | 3.3 | 2.7 |
| Ta | 0.10 | 0.06 | 0.17 | 0.32 | 0.64 | 1.36 | 0.66 | 0.71 | 0.94 | 0.53 | 0.31 | 0.22 | 0.20 | 0.18 | 0.34 | 0.27 | 0.20 | 0.19 | 0.27 | 0.33 | 0.68 | 0.37 |
| W | 24.7 | 16.1 | 1.4 | 1.7 | 1.3 | 0.32 | 0.89 | 1.2 | 1.9 | 0.52 | 0.68 | 0.74 | 0.99 | 1.9 | 4.1 | nd | 3.4 | 6.7 | < 1 | 1.01 | 3.9 | 1.17 |
| Th | 4.2 | 0.78 | 2.4 | 5.2 | 11.3 | 6.2 | 13.8 | 10.6 | 9.6 | 4.19 | 5.17 | 5.11 | 2.9 | 2.7 | 5.4 | 2.7 | 2.9 | 2.3 | 4.9 | 7.2 | 6.7 | 6.7 |
| U | 0.2 | 0.5 | 1.0 | 1.0 | 1.9 | 1.1 | 1.5 | 1.2 | 1.5 | 0.65 | 1.11 | 0.76 | 0.78 | 0.96 | 1.1 | 1.0 | 0.76 | 0.81 | 1.65 | 1.95 | 0.93 | 1.11 |

| KM-112 | KM-113 | KM-114 | KM-115 | KM-116 | KM-127 | KM-128 | KM-129 | KM-131 | KM-144 | KM-148 | KM-149 | KM-150 | KM-152 | KM-153 | KM-154 | KM-155 | KM-156 | KM-157 | KM-158 | KM-159 | KM-160 |
|---|---|---|---|---|---|---|---|---|---|---|---|---|---|---|---|---|---|---|---|---|---|
| 0.24 | 0.36 | 0.70 | 0.13 | 2.37 | 0.20 | 0.27 | 3.60 | 2.72 | 0.27 | 4.86 | 3.77 | 2.83 | 4.95 | 1.65 | 0.35 | 0.43 | 0.82 | 1.69 | 5.36 | 0.59 | 0.60 |
| 0.59 | 0.68 | 0.58 | 0.62 | 0.81 | 1.16 | 0.92 | 1.17 | 0.99 | 1.18 | 1.44 | 1.26 | 1.38 | 0.84 | 0.67 | 1.65 | 1.46 | 0.96 | 0.84 | 0.63 | 1.0 | 1.1 |
| 1.2 | 1.8 | 1.4 | 1.0 | 7.3 | 9.7 | 6.9 | 2.0 | 12.2 | 15.8 | 2.9 | 2.7 | 3.7 | 5.1 | 0.8 | 6.2 | 1.8 | 4.7 | 10.9 | 2.2 | 7.2 | 6.0 |
| 13.4 | 8.6 | 9.74 | 14.47 | 44.8 | 37.3 | 10.77 | 1.657 | 7.17 | 3.95 | 2.02 | 2.67 | 2.86 | 3.94 | 1.8 | 4.07 | 2.53 | 1.94 | 1.53 | 1.4 | 7.4 | 5.8 |
| 145 | 199 | 132 | 126 | 158 | 61 | 143 | 42.6 | 113.4 | 121 | 35.2 | 29 | 47.8 | 150 | 23.6 | 68.8 | 167 | 61.2 | 133.4 | 42 | 202 | 231 |
| 12.2 | 6.1 | 9.11 | 26.57 | 6.77 | 3.70 | 3.20 | 20.80 | 7.50 | 8.91 | < 0.5 | 10.90 | 9.20 | 7.40 | 14.20 | 8.50 | 16.78 | 26.00 | 7.3 | 1.8 | 4.9 | 7.7 |
| 0.94 | 0.67 | 0.79 | 0.90 | 0.84 | 0.73 | 0.87 | nd | 2.50 | 0.65 | 0.52 | 0.67 | 0.34 | 1.16 | 0.61 | 0.44 | 1.55 | 0.77 | 0.61 | nd | 0.89 | 0.95 |
| 346 | 219 | 303 | 284 | 295 | 467 | 469 | 374 | 330 | 854 | 141 | 315 | 359 | 300 | 384 | 461 | 410 | 704 | 263 | 93 | 662 | 588 |
| 45 | 108 | 211 | 416 | 217 | nd | 86 | 157 | 465 | 68 | 449 | 382 | 599 | 417 | 99 | 73 | 118 | 106 | 166 | 491 | 45 | 168 |
| 0.26 | 0.29 | 0.18 | 0.20 | 0.29 | 0.36 | 0.19 | 0.33 | 0.31 | 0.35 | 0.06 | 0.40 | 0.39 | 0.24 | 2.6 | 7.7 | 3.1 | 0.58 | 0.43 | 0.23 | 1.8 | 2.9 |
| 10.9 | 6.8 | 5.5 | 11.1 | 20.8 | 19.1 | 22.8 | 2.1 | 20.1 | 146 | 2.2 | 2.5 | 18.6 | 8.3 | 2.1 | 16.0 | 13.3 | 5.9 | 67.8 | 13.9 | 23.8 | 48.2 |
| 1336 | 6402 | 8510 | 38 899 | 991 | 950 | 935 | 481 | 926 | 594 | 704 | 1068 | 894 | 829 | 1044 | 800 | 1256 | 1859 | 415 | 674 | 2622 | 1385 |
| 9.02 | 7.93 | 10.0 | 9.8 | 11.9 | 15.1 | 20.9 | 32.2 | 26.1 | 23.6 | 27.5 | 33.4 | 27.7 | 55.8 | 23.2 | 16.0 | 39.7 | 25.09 | 27.1 | 19.7 | 20.6 | 37.8 |
| 28.0 | 46.7 | 23.9 | 20.2 | 31.8 | 57.9 | 63.7 | 91.0 | 53.8 | 67.8 | 103.4 | 78.2 | 65.2 | 103.5 | 83.9 | 34.7 | 66.4 | 53.0 | 59.9 | 31.2 | 55.8 | 94.1 |
| 4.3 | 3.9 | 8.1 | 3.8 | 5.8 | 17.5 | 20.5 | 33.5 | 22.0 | 24.6 | 28.4 | 27.1 | 24.6 | 49.9 | nd | 15.2 | 16.9 | 20.4 | 21.6 | 7.4 | 22.5 | 34.5 |
| 1.2 | 1.1 | 1.4 | 1.6 | 1.4 | 3.7 | 4.2 | 7.4 | 4.7 | 5.3 | 7.6 | 5.9 | 5.3 | 10.8 | 7.1 | 4.4 | 3.5 | 4.5 | 5.3 | 1.3 | 5.0 | 7.8 |
| 0.29 | 0.28 | 0.44 | 0.48 | 0.51 | 0.82 | 0.81 | 1.32 | 1.7 | 0.78 | 1.6 | 2.0 | 1.7 | 2.6 | 0.96 | 1.06 | 0.62 | 1.12 | 1.2 | 0.68 | 1.0 | 1.7 |
| 0.22 | 0.17 | 0.30 | 0.63 | 0.32 | 0.54 | 0.53 | 1.16 | 0.72 | 0.69 | 1.4 | 1.0 | 0.8 | 1.7 | 1.6 | 1.5 | 0.39 | 0.59 | 0.79 | 0.18 | 1.0 | 1.1 |
| 0.88 | 0.62 | 1.3 | 2.3 | 1.91 | 1.29 | 1.28 | 3.87 | 2.2 | 1.60 | 5.0 | 3.3 | 2.5 | 4.0 | 5.6 | 5.1 | 1.2 | 1.9 | 2.2 | 1.0 | 3.9 | 3.6 |
| 0.14 | 0.10 | 0.19 | 0.30 | 0.29 | 0.16 | 0.18 | 0.57 | 0.30 | 0.21 | 0.74 | 0.47 | 0.34 | 0.54 | 0.72 | 0.71 | 0.18 | 0.27 | 0.31 | 0.15 | 0.56 | 0.53 |
| 1.4 | 1.4 | 1.7 | 2.09 | 2.7 | 1.6 | 2.2 | 4.8 | 2.5 | 2.6 | 6.5 | 3.0 | 3.3 | 3.7 | 1.8 | 3.3 | 2.4 | 4.8 | 3.0 | 2.4 | 2.7 | 2.7 |
| 0.20 | 0.22 | 0.18 | 0.23 | 0.24 | 0.13 | 0.18 | 1.16 | 0.40 | 0.22 | 1.5 | 0.60 | 0.86 | 0.23 | 0.42 | 0.45 | 1.09 | 0.39 | 0.39 | 0.39 | 0.30 | 0.33 |
| 1.73 | 2.40 | nd | nd | nd | nd | 2.9 | 0.5 | 35.8 | 2.5 | 11.8 | 16.1 | 45.0 | 2.2 | 6.4 | 3.6 | 4.0 | 3.6 | 1.9 | 0.90 | 4.9 | 2.7 |
| 3.7 | 2.2 | 3.3 | 3.4 | 4.7 | 2.1 | 2.3 | 14.5 | 3.5 | 4.8 | 17.3 | 9.2 | 6.5 | 3.0 | 5.5 | 5.9 | 17.6 | 3.7 | 4.0 | 9.8 | 4.3 | 3.6 |
| 0.85 | 0.59 | 0.77 | 1.6 | 2.4 | 0.59 | 0.61 | 2.6 | 0.84 | 0.80 | 3.2 | 2.0 | 1.0 | 1.5 | 0.97 | 1.1 | 4.8 | 1.0 | 1.9 | 1.6 | 1.3 | 1.2 |

from each unit, were compared to altered samples from their respective eruptive units. Sample KJH-26 consists of separated plagioclase crystals from an unaltered Hells Mesa Tuff sample. For the upper Lemitar Tuff, sample KM-148 is used as the unaltered separated sample. Although KM-148 has undergone a small degree of alteration, we feel the very slight alteration that has taken place has no material effect on the conclusions presented in this paper. Geochemical analytical results for the separated samples are shown in Table 5.

When compared to the chemistry of the separated samples KM-148 and KJH-26, several elements in the separated samples show consistently elevated concentrations including Sc, Co, Zn, As, Br, Rb, Sb, Cs, and Ba (Fig. 8). This figure does not reflect As enrichment or depletion because this element was not detected ($< 0.5$ ppm) in either KJH-26 or KM-148. However, As is interpreted to be enriched upon alteration as indicated by the relatively high values found in the separated samples. The concentration of Ba was found to vary dramatically between 112 to 38,900 ppm for the two units.

Elements showing significant depletion include $Na_2O$, Sr, and Eu; all elements compatible in plagioclase (McBirney, 1993; Fig. 8). $Na_2O$ within the

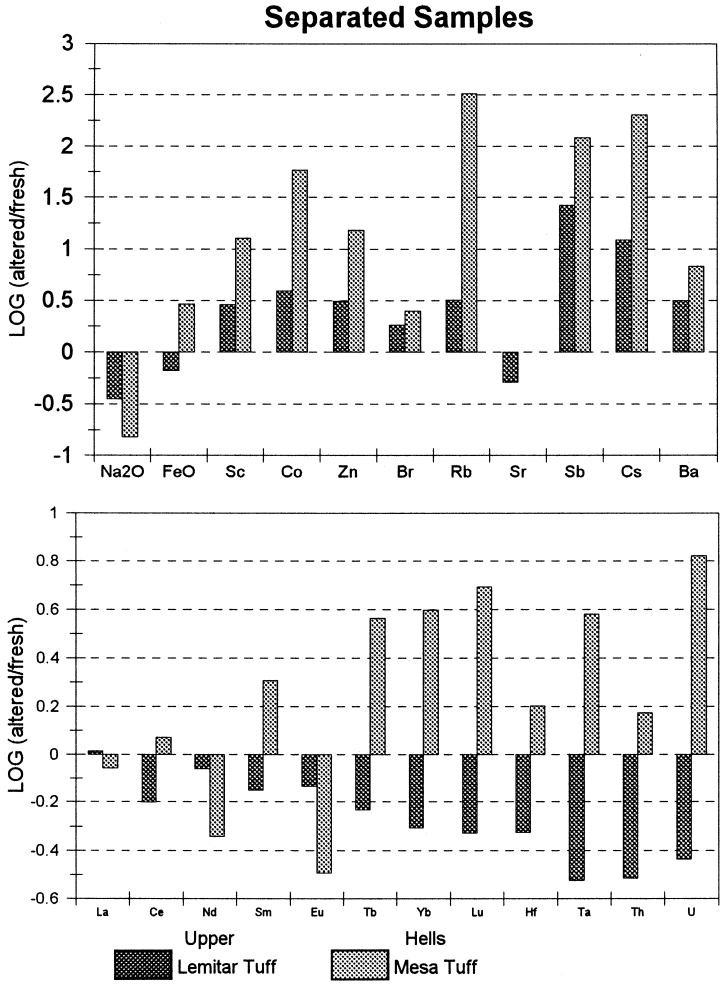


Fig. 8. Enrichment/depletion diagrams for elements within the separated samples of the upper Lemitar and Hells Mesa Tuffs. Unaltered samples used to calculate the enrichment/depletion factors were KM-148 (upper Lemitar Tuff) and KJH-26 (Hells Mesa Tuff).

separated samples of both units ranges from 0.10 to 5.36 wt.% with KJH-26 containing 6.86 wt.% and KM-148 having 4.86 wt.% $Na_2O$. Values for Sr in the separated samples range from 35 to 599 ppm. KJH-26 was not analyzed for Sr, therefore an enrichment or depletion factor was not calculated for Hells Mesa Tuff separated samples on Fig. 8. KM-148 contains 449 ppm Sr and reflects overall depletion of Sr within the upper Lemitar Tuff.

As with whole rock samples, several elements show markedly different trends between the two tuffs. For instance, the elements Fe, La, Ce, Sm, Tb, Yb, Lu, Hf, Ta, Th, and U, are depleted within upper Lemitar Tuff separated samples when compared to KM-148, but are enriched within Hells Mesa Tuff separated samples when compared to KJH-26 (Fig. 8). The enrichment of these elements within the upper Lemitar Tuff separated samples and the depletion within the Hells Mesa Tuff separated samples is similar to the trends found in whole rock analyses (compare Figs. 7 and 8).

## 3. Discussion

### *3.1. Major and trace elements*

K-metasomatic alteration resulted in significant deviation from the primary chemistry of the upper Lemitar and Hells Mesa ignimbrites. Notably, samples from this study are significantly enriched in $K_2O$, Rb, As, Ba, Pb, Sb, and Cs and depleted in $Na_2O$, CaO, and Sr (Figs. 7 and 8). The enrichment or depletion of many of these elements has been recognized by Chapin and Lindley (1986) and Dunbar et al. (1994). The lack of significant deviation for $TiO_2$ and $Al_2O_3$ indicates no significant mass loss or gain within the units, suggesting the trends seen in other elements represent true rather than apparent chemical changes in the rock. As discussed previously, $Na_2O$ depletion and $K_2O$ enrichment is a result of plagioclase dissolution and adularia formation. MgO depletion is noted by Dunbar et al. (1994) in silicic ignimbrites, however, only the Hells Mesa Tuff shows minor depletion in this study.

Elements such as $K_2O$ and Rb appear to be controlled primarily by the stability of the alteration assemblage produced upon plagioclase dissolution. In contrast, $Na_2O$ and Sr are depleted as a result of plagioclase instability and are removed from the system upon alteration. The observation that the chemical changes reflect the alteration mineral assemblage is supported by the greater relative increase in the enrichment/depletion factors calculated for the separated samples compared to whole rock samples.

Several elements, including As, Sb, Ba, and Pb, display anomalous enrichments that are geographically associated with known areas of hydrothermal alteration and mineralization. For instance, when the concentration of As in over 200 K-metasomatized samples is contoured, there is a broad As enrichment of approximately 5 ppm over the entire K-metasomatized area, but superimposed upon this are sharp concentration spikes centered on areas where high-temperature hydrothermal activity has been recognized (Dunbar et al., 1995). These anomalous values contribute significantly to the enrichment factors calculated for As and Sb in Fig. 7, especially for the upper Lemitar Tuff. It is also likely that samples containing high concentrations of Ba represent samples affected by hydrothermal alteration as many Ba-enriched samples are found either associated with the Luis Lopez manganese district, or with Mn-mineralized areas on the east side of the Magdalena Mountains (Fig. 1). A small number of Hells Mesa Tuff samples collected from Socorro Peak, an area of fairly intense hydrothermal alteration resulting in galena mineralization with extensive secondary barite (Lasky, 1932), have considerably elevated Pb and Ba concentrations, suggesting the enrichment factors for these elements calculated for Fig. 7 are not a result of K-metasomatism. Low level increases of As and possibly Ba and Sb enrichment appear to be related to K-metasomatism, however, high levels appear attributable to hydrothermal alteration.

### *3.2. Rare earth elements*

Depletion of REE in the upper Lemitar Tuff and enrichment in the Hells Mesa Tuff observed in this study is unique, for most studies of K-metasomatism report little to no variation in REE distribution as a result of alteration (i.e., Glazner, 1988; Roddy et al., 1988; Hollocher et al., 1994). Some researchers believe that movement of fluids during diagenesis has

the ability to change REE distributions and ratios (i.e., Alderton et al., 1980; Condie et al., 1995), however, others believe diagenetic and low-grade metamorphic effects on REE are minimal (i.e., Chaudhaui and Cullers, 1979; Elderfield and Sholkovitz, 1987; Sholkovitz, 1988), especially when the fluid temperature is $< 230°C$ (Michard, 1988). In this study, the separated sample REE trends reflect those seen in whole rock samples, but are distinctly more pronounced suggesting that variation in REE content may be a function of alteration mineralogy produced by the metasomatic process.

A possible mechanism through which REE may have been depleted in the upper Lemitar Tuff and enriched in the Hells Mesa Tuff is through re-equilibration between the mineral assemblage and the altering fluid. Trace element analyses indicates that unaltered plagioclase from the upper Lemitar Tuff is approximately 1.2 to 3.0 times greater in LREE (La, Ce, and Nd) content and 6.6 to 11 times greater in middle and HREE (Sm to Lu, excluding Eu) content compared to plagioclase from the Hells Mesa Tuff. This substantial difference between the middle and HREE content of plagioclase from the two units may explain why enrichment or depletion of middle and HREE is particularly striking while LREE show variable concentrations. Data indicate a convergence toward similar REE contents upon alteration, suggesting an equilibrium fluid REE concentration approximately intermediate to the REE content of upper Lemitar and Hells Mesa Tuff plagioclase (Fig. 9). Because the difference between the LREE content of plagioclase from the two units is relatively minor, a fluid of an intermediate composition would not likely cause a significant change in the LREE content upon re-equilibration. Initial results from this study, however, appear to indicate that re-equilibration between the fluid and alteration mineral assemblage may be a viable mechanism to explain the REE contents of the separated samples. Preliminary

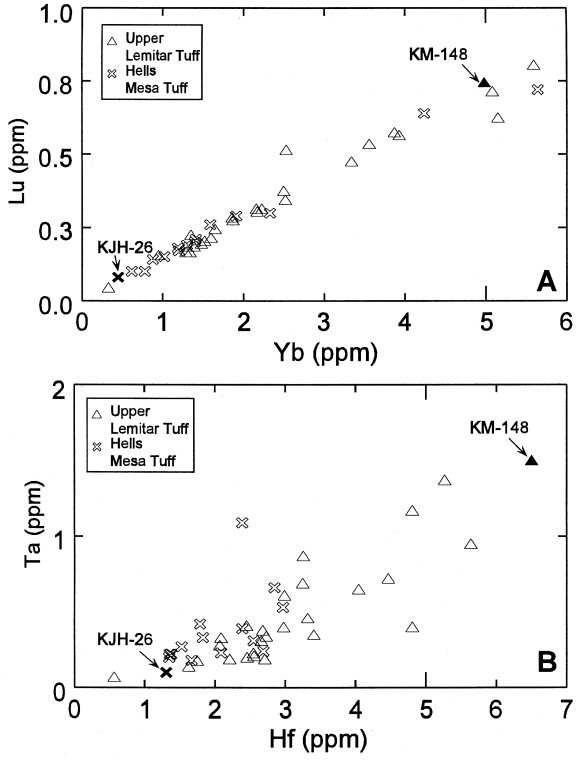


Fig. 9. (A and B) Heavy rare earth element and trace element trends in separated samples compared to unaltered plagioclase (KM-148 and KJH-26).

data from the Socorro K-anomaly also suggest that clay minerals may play a significant role in incorporating REE and may provide the mechanism for REE redistribution during K-metasomatism (Ennis, 1996).

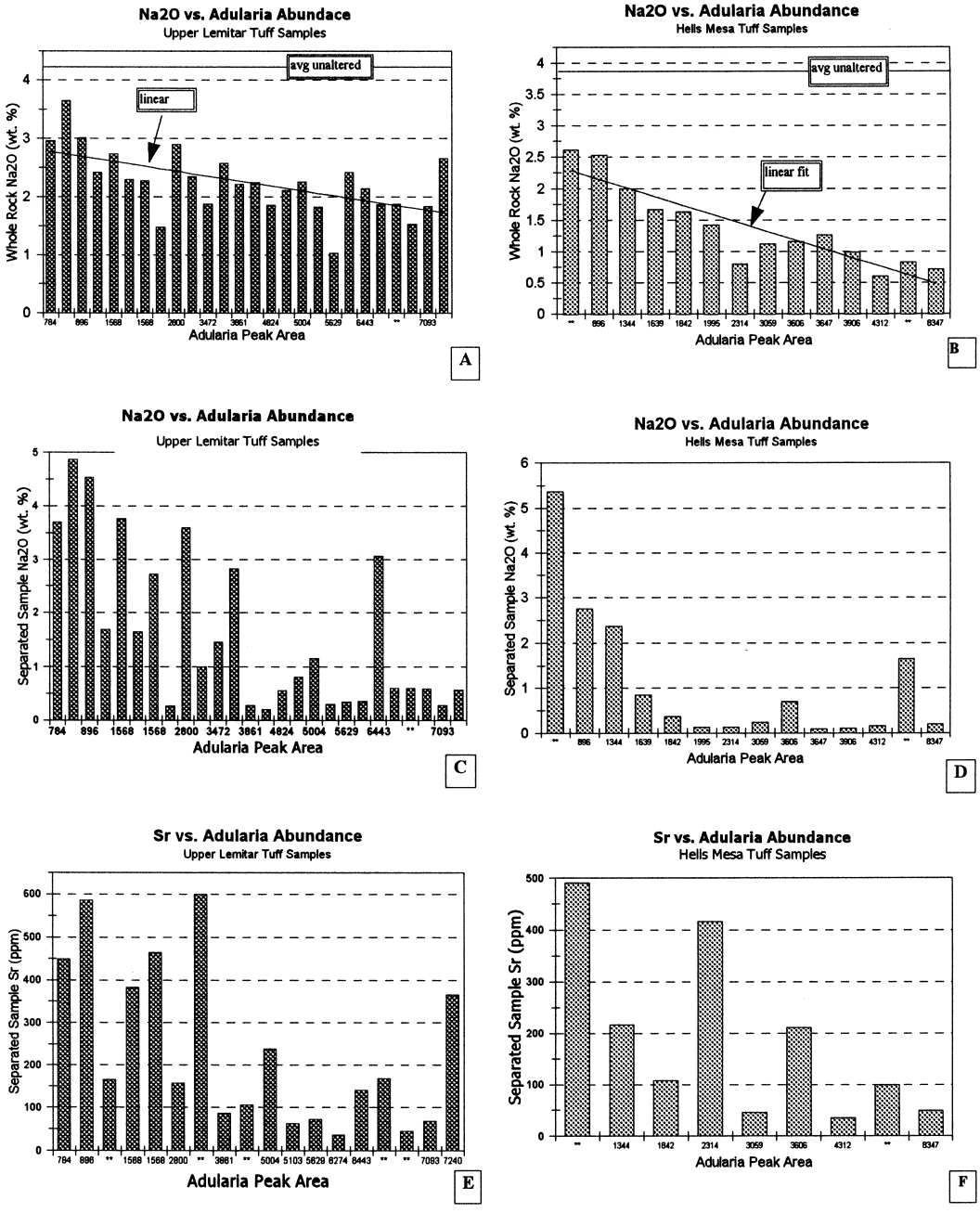


Fig. 10. (A–F) Increasing adularia peak area (adularia abundance) within separated samples vs. whole rock $Na_2O$ (A and B), $Na_2O$ in separated samples (C and D), and Sr in separated samples (E and F) for the upper Lemitar and Hells Mesa Tuffs. * * Indicates samples where peak area was estimated based on similar XRD patterns.

### 3.3. Mineralogy and geochemistry

#### 3.3.1. Residual mineral phases

*3.3.1.1. Plagioclase.* Plagioclase phenocrysts in the upper Lemitar and Hells Mesa Tuffs were replaced by a mineral assemblage dominantly composed of adularia, quartz, and a variety of clay minerals. Although clay minerals such as smectite and kaolinite commonly replace plagioclase during diagenesis and weathering, unmetasomatized upper Lemitar and Hells Mesa Tuff samples examined in this section contain unaltered plagioclase with no significant signs of replacement.

During K-metasomatism, plagioclase is chemically unstable but remains in the mineral assemblage as a result of incomplete dissolution during alteration. Plagioclase dissolution during K-metasomatism caused a marked decrease in $Na_2O$ and Sr content in both whole rock and separated samples. A negative correlation is observed between adularia abundance in altered whole rock samples and $Na_2O$ content (Fig. 10a and b). $Na_2O$ depletion in the separated samples is also evident and elucidates the process by which $Na_2O$ depletion takes place during alteration (Fig. 10c and d). Within the separated samples, $Na_2O$ content decreases dramatically with increasing adularia abundance, presumably as a result of plagioclase dissolution. As such, increasing adularia abundance should vary inversely with the amount of residual plagioclase contained within a sample. The amplified $Na_2O$ depletion in separated samples is due to the dilution effect caused by the presence of other $Na_2O$ bearing phases within whole rock samples which are less easily altered than plagioclase. The Sr content of both whole rock and separated samples correlates with $Na_2O$ content due to Sr compatibility in plagioclase (Fig. 10e and f).

#### 3.3.2. Mineral phases related to K-metasomatism

*3.3.2.1. Adularia.* The dominant phase produced by metasomatic alteration is adularia. Adularia has been observed in a number of other tuffaceous rock units that have undergone alkaline–saline brine alteration, such as in Jurassic lake T'oo'dichi (Turner and Fishman, 1991) the Green River Formation in Wyoming (Surdam and Parker, 1972), and in tuffs in Arizona (Brooks, 1986). Based on SEM observations, adularia is produced through the alteration of plagioclase, and is characteristically euhedral. Based on the chemical composition of the samples, the transformation from plagioclase to adularia appears to be relatively simple exchange of K for Na. This reaction assumes an albite endmember composition for plagioclase, which is reasonable based on electron microprobe data from the two volcanic units (Ennis, 1996). Assuming that the plagioclase con-

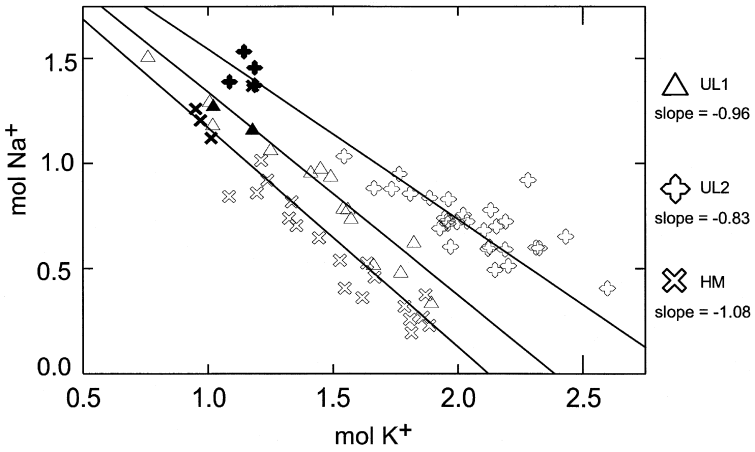


Fig. 11. mol $K^+$ vs. mol $Na^+$ for upper Lemitar and Hells Mesa Tuff whole rock samples. Upper Lemitar samples show two trends (UL1 and UL2) due to compositional zonation, while the Hells Mesa Tuff only shows one. Closed symbols indicate unaltered samples collected outside of the K-metasomatized anomaly.

tains little Ca, the K:Na ratio this type of reaction should approximate 1:1, which is confirmed by geochemical results from this study (Fig. 11). This figure shows trends for the Hells Mesa and Lower Lemitar Tuffs, showing evidence of close to a 1:1 exchange of Na for K. The reason for the three distinct trends shown on the figure is that the initial Na:K ratios for the Hells Mesa, and two different sample groups of the Upper Lemitar are different (see the unaltered compositions on the figure), giving different starting points to the regression lines. Based on dissolution textures observed in partially altered plagioclase crystals (Fig. 6), as well as euhedral adularia crystals observed on a plagioclase substrate (Fig. 2), the adularia appears to form by a dissolution–precipitation reaction.

When samples are ranked based on increasing adularia abundance, several chemical trends are apparent. In general, an increase in the adularia content of the upper Lemitar and Hells Mesa ignimbrites corresponds to an increase in whole rock $K_2O$ and Rb content (Fig. 12a and b). The increase in Rb concentration is likely due to substitution for K in adularia (Fig. 12c and d; Deer et al., 1992). Whole rock Hells Mesa Tuff samples show a 2-fold increase in Rb content while separated samples show a striking 10-fold increase when compared to unaltered material. The dramatic Rb increase of the Hells Mesa Tuff separated samples when compared to whole rock samples suggests that minerals in the secondary alteration assemblage, particularly adularia, strongly influence the concentration of Rb.

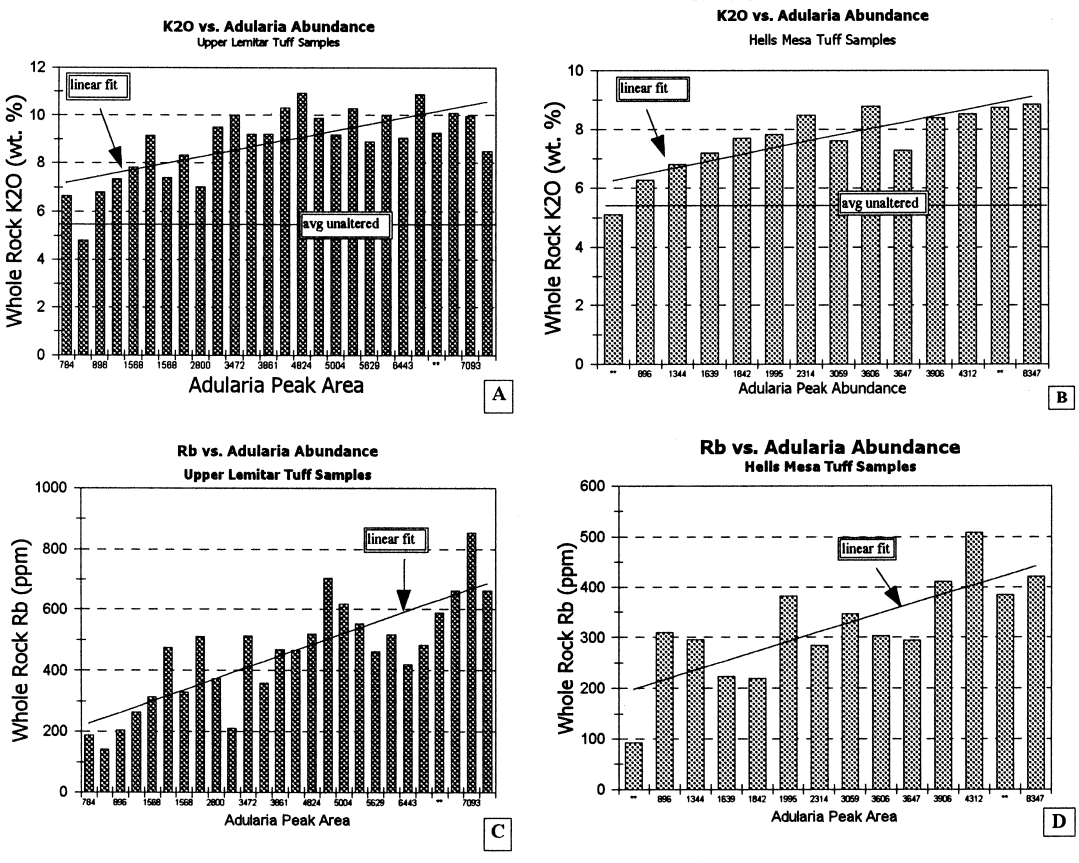


Fig. 12. (A–D) Increasing adularia peak area (adularia abundance) within separated samples vs. whole rock $K_2O$ (A and B) and Rb (C and D) content for the upper Lemitar and Hells Mesa Tuffs. * * Indicates samples where peak area was estimated based on similar XRD patterns.

*3.3.2.2. Illite, smectite, and mixed-layer I/S.* Mixed-layer I/S is one of the most common clay minerals present within the Socorro K-metasomatized area, whereas discrete smectite and illite are rare in the alteration assemblage. The smectite observed is though to be a product of the early stages of metasomatism, when the $K^+/H^+$ of the metasomatic fluid is low. Smectite is known to form in alkaline, saline environments (i.e., Jones and Weir, 1983; Hay and Guldman, 1987; de Pablo-Galan, 1990), but smectite cannot form in the presence of a high K fluid (Deer et al., 1992). However, if the metasomatizing fluid had a relatively low cation/$H^+$ activity ratio, precipitation of smectite associated with plagioclase dissolution may occur (Duffin et al., 1989; Harrison and Tempel, 1993). As the fluid increased in $K^+/H^+$ ratio and/or temperature, due to progressive evaporation of the lake brine, the formation of smectite would cease. At this point, formation of mixed-layer I/S could occur as a result of illitization involving addition of K to smectite. The reaction that causes illitization of smectite releases silica (Boles and Franks, 1979), which may also explain some of the fine-grained quartz within the alteration assemblage. A fluid-mediated reaction such as illitization may be governed by three processes: dissolution, solute mass transfer, and precipitation or crystallization (Eberl and Srodon, 1988). The fine-grained nature of the primary smectite and the sheet-like morphology of the grains significantly increase the rate of dissolution, allowing extensive cationic substitution within the smectite (May et al., 1986; Whitney, 1990). K-metasomatism in the Socorro area was presumably fluid-dominated with an abundance of ions as indicated by the extensive addition of K throughout the anomaly. The high K concentration in the fluid would cause smectite to become illitized by K fixation between the smectite layers (Jones and Weir, 1983; Awwiller, 1993). The temperature required for transformation of smectite to mixed-layer I/S occurs at temperatures of 100°C or less (e.g., Aoyagi and Kazama, 1980), although illitization has been reported at lower temperatures (Jones and Weir, 1983; Srodon and Eberl, 1984). These temperature estimates are similar to the temperatures at which K-metasomatism is thought to have occurred in the Socorro area (Chapin and Lindley, 1986; Dunbar et al., 1996). An alternative mechanism for formation of mixed layer I/S is by breakdown of K-feldspar. This process is frequently called upon to form illite and/or mixed-layer I/S in diagenetic settings (i.e., Boles and Franks, 1979; Altaner, 1986; Wintsch and Kvale, 1994). However, in the case of the Socorro K-metasomatism, mixed layer I/S is associated with plagioclase, rather than K-feldspar.

### *3.3.3. Mineral phases related to hydrothermal alteration*

*3.3.3.1. Kaolinite*. Kaolinite is an extremely common clay mineral in the alteration assemblage of samples collected within the K-anomaly. SEM photographs clearly demonstrate the euhedral morphology of kaolinite, indicating an authigenic origin, however, the mechanism through which kaolinite formed in these samples is somewhat difficult to ascertain.

Within the Socorro K-anomaly, presence of kaolinite in the alteration assemblage tends to coincide with areas of hydrothermal alteration, suggesting a hydrothermal source for kaolinite within the assemblage. For example, Hells Mesa Tuff samples KM-112 through KM-116 were collected near the Luis Lopez manganese district and contain kaolinite as the dominant clay mineral in the secondary assemblage (Table 1). Kaolinite is recognized in many types of hydrothermal alteration such as argillic and advanced argillic due to wall–rock interaction. In these regimes, kaolinite formation is restricted to lower temperatures ($< 200$°C), indicating its formation during the late stages of hydrothermal activity (Guilbert and Park, 1986). Hydrothermal kaolinite typically exhibits a characteristic texture of tightly packed small flakes which tend to occur as single sheets, sheaves, or thin packets rather than expansive books (Keller, 1976). This is similar to the kaolinite morphology observed through SEM analysis in this study. Additionally, kaolinite formation during diagenesis occurs under dilute, acidic conditions while basic and concentrated solutions result in kaolinite instability (Dunoyer de Segonzac, 1970).

Conditions for K-metasomatism in the Socorro area are believed to have been alkaline, (Chapin and Lindley, 1986), again implying kaolinite was formed as a product of hydrothermal events superimposed

on the Socorro K-anomaly. The presence of barite in the separated sample of KM-115, as well as elevated Ba content in several other samples, further suggests some amount of hydrothermal overprinting.

### 3.4. Summary

K-metasomatism near Socorro, New Mexico has affected the geochemical and mineralogical composition of Cenozoic rocks including two silicic ignimbrites, the upper Lemitar and Hells Mesa, which were investigated in this study. K-metasomatism strongly affected Na-rich minerals, particularly plagioclase, while K-rich minerals are basically unaffected during alteration. Using XRD and semi-quantitative clay mineral analysis, the alteration assemblage was found to consist of various amounts of adularia, quartz, mixed-layer I/S, kaolinite, discrete smectite and illite, and minor calcite and barite. Some residual plagioclase remains in the assemblage as a result of incomplete dissolution during K-metasomatism. Kaolinite and mixed-layer I/S are the most common clay minerals present within the altered plagioclase. Discrete smectite and illite occur infrequently in the alteration assemblage. SEM and electron microprobe data from this study suggest the alteration assemblage formed through a dissolution–precipitation reaction as indicated by the presence of dissolution textures within plagioclase phenocrysts and mixed-layer clay in the assemblage.

It is probable that mixed-layer I/S, discrete smectite and illite were formed during K-metasomatism as a result of changes in the fluid chemistry. Smectite may have formed during stages of metasomatism when the fluid was relatively dilute and had a low cation/$H^+$ ratio. As the fluid became progressively more concentrated in $K^+$, it is likely that smectite illitization occurred resulting in the formation of mixed-layer clays. Kaolinite is most likely the result of hydrothermal overprinting as indicated by a strong correlation between areas of known hydrothermal activity and large abundances of kaolinite in the alteration assemblage. Kaolinite formation is also promoted by acidic conditions suggesting it is not likely to have formed under the alkaline conditions imposed during K-metasomatic alteration, thus, further supporting a hydrothermal origin for this mineral. Calcite, which is extremely rare in the alteration assemblage, is fine-grained and likely formed as a result of plagioclase dissolution. Barite is present in the assemblage due to localized hydrothermal events in the Socorro area.

The detailed study of altered plagioclase reveals the presence of a clay mineral, kaolinite that should not have formed during an alkaline–saline alteration event. The presence of this mineral helped unravel the complex chemical changes that took place due to several episodes of hydrothermal alteration. We also interpret that the enrichment of some elements in altered rocks is related to the hydrothermal events that produced kaolinite. Without the recognition of the origin of kaolinite, enrichment of some elements in altered rocks could have been incorrectly attributed to K-metasomatism.

The chemical composition of altered rocks shows overall enrichment of $K_2O$, Rb, Ba, As, Sb, Cs, and Pb along with marked depletion of $Na_2O$, CaO, and Sr when compared to unmetasomatized samples. Enrichment of $K_2O$ and Rb in whole rock samples correlates positively with the abundance of adularia in the separated, altered plagioclase samples. A strong negative correlation is also shown for $Na_2O$ and Sr content with increasing adularia content in the separated samples due to plagioclase dissolution during the alteration process. The separated samples typically show the biggest chemical effects, which tend to be diluted in whole rock samples.

Enrichment of Ba, As, Sb, Cs, and Pb in the two ignimbrites is likely a result of input from a hydrothermal source as demonstrated by a correlation between high concentrations of these elements in samples collected near areas of hydrothermal overprinting. Low levels of As and possibly Ba and Sb enrichment, however, appear to be related to K-metasomatism.

Other elements showing enrichment/depletion include the middle and HREE. Enrichment of middle and HREE in the upper Lemitar Tuff and depletion in the Hells Mesa Tuff suggests attempted re-equilibration between the secondary alteration assemblage and the alteration fluid. Evidence suggests the fluid REE content was intermediate to the REE concentrations found within upper Lemitar and Hells Mesa Tuff plagioclase, which would account for

both enrichment and depletion within the two units. Preliminary data suggest clay minerals may have played an important role during redistribution and may have provided the necessary binding sites for REE.

This study documents enrichments and depletions of many elements in rocks altered by K-metasomatism. Calculations suggest that $6.4 \times 10^{10}$ tons of K have been added to the Socorro K-metasomatized area (Chapin and Lindley, 1986), and many tons of other elements have been depleted. The K that has been added to the rocks could be leached from rocks in a very wide geographic area, concentrated in playa fluids by evaporation, and then added to the Socorro area rocks. Hoch et al. (1999) describe how high K waters can be produced from weathering of freshly exposed surfaces on ash flow tuffs, and a similar mechanism may produce K-rich fluids in the Socorro area. If the K-rich fluids were produced by this mechanism, no distinct K-poor source area could be recognized in the Socorro area, and none is.

## Acknowledgements

Funding for this project was provided by the National Science Foundation (EAR-9219758 to A.R.C. and C.E.C.), the New Mexico Bureau of Mines and Mineral Resources, and the New Mexico Geological Society. We would like to thank Philip Kyle, Peter Mozley, Richard Chamberlin, George Austin, Chris McKee and Mike Spilde for discussion, support, and constructive suggestions. We would like to thank J.I. Drever, K. Hollocher, and an anonymous reviewer for insightful review of the manuscript. XRF analysis was performed at the New Mexico Institute of Mining and Technology X-ray Fluorescence Facility for which partial funding was provided by National Science Foundation Grant EAR93-16467. *[JD]*

## References

Alderton, D., Pearce, J., Potts, P., 1980. Rare earth mobility during granite alteration: evidence from southwest England. Earth and Planetary Science Letters 49, 149–165.

Altaner, S., 1986. Comparison of rates of smectite illitization with rates of K-feldspar dissolution. Clays and Clay Minerals 5, 608–611.

Aoyagi, K., Kazama, T., 1980. Transformational changes of clay minerals, zeolites, and silica minerals during diagenesis. Sedimentology 27, 179–188.

Austin, G.S., Leininger, R.K., 1976. Effects of heat-treating mixed-layer illite–smectite as related to quantitative clay mineral determinations. Journal of Sedimentary Petrology 46, 206–215.

Awwiller, D.N., 1993. Illite/smectite formation and potassium mass transfer during burial diagenesis of mudrocks: a study from the Texas Gulf Coast Paleocene–Eocene. Journal of Sedimentary Petrology 63, 501–512.

Boles, J.R., Franks, S.G., 1979. Clay diagenesis in Wilcox Sandstones of Southwest Texas: implications of smectite diagenesis on sandstone cementation. Journal of Sedimentary Petrology 49, 55–70.

Brooks, W.E., 1986. Distribution of anomalously high $K_2O$ volcanic rocks in Arizona: metasomatism at the Picacho Peak detachment fault. Geology 14, 339–342.

Chamberlin, R.M., 1980. Cenozoic stratigraphy and structure of the Socorro Peak volcanic center, central New Mexico. PhD Thesis, Colorado School Mines, Golden.

Chapin, C.E., Chamberlin, R.M., Osburn, G.R., White, D.W., 1978. Exploration framework of the Socorro geothermal area. New Mexico Geological Society Special Publication 7, 115–130.

Chapin, C.E., Lindley, J.I., 1986. Potassium metasomatism of igneous and sedimentary rocks in detachment terranes and other sedimentary basins: economic implications. Arizona Geological Society Digest XVI, 118–126.

Chaudhaui, S., Cullers, R.L., 1979. The distribution of REE in deeply buried Gulf Coast sediments. Chemical Geology 24, 327–338.

Condie, K.C., Dengate, J., Cullers, R.L., 1995. Behavior of rare earth elements in a paleoweathering profile on granodiorite in the Front Range, Colorado, USA. Geochimica Cosmochimica Acta 59, 279–294.

D'Andrea, J.F., 1981. The geochemistry of the Socorro anomaly, New Mexico, Thesis, Florida State University, 243 pp.

Davis, G.A., Lister, G.S., Reynolds, S.J., 1986. Structural evolution of the whipple and south mountains shear zones, Southwestern United States. Geology 14, 7–10.

Deer, W.A., Howie, R.A., Zussman, J., 1992. In: An Introduction to the Rock Forming Minerals, 1. Longman Group, London, p. 528.

de Pablo-Galan, L., 1990. Diagenesis of oligocene–miocene vitric tuffs to montmorillonite and K-feldspar deposits, Durango, Mexico. Clays and Clay Minerals 38, 426–436.

Duffin, M.E., Lee, M.C., Klein, G.D., Hay, R.L., 1989. Potassic diagenesis of Cambrian sandstones and Precambrian granitic basement in the UPH-3 deep hole, Upper Mississippi Valley, USA. Journal of Sedimentary Petrology 59, 848–861.

Dunbar, N.W., Chapin, C.E., Ennis, D.J., 1995. Arsenic enrichment during potassium metasomatism and hydrothermal pro-

cesses in the Socorro, NM area-implications for tracing groundwater flow. New Mexico Geology 17, 26.

Dunbar, N.W., Chapin, C.E., Ennis, D.J., Campbell, A.R., 1994. Trace element and mineralogical alteration associated with moderate and advanced degrees of K-metasomatism in a rift basin at Socorro, New Mexico. New Mexico Geological Society Guidebook 45, 225–232.

Dunbar, N.W., Kelley, S., Miggins, D., 1996. Chronology and thermal history of potassium metasomatism in the Socorro, NM, area: Evidence from $^{40}Ar/^{39}Ar$ dating and fission track analysis. New Mexico Geology 18, 50.

Dunoyer de Segonzac, G., 1970. The transformation of clay minerals during diagenesis and low-grade metamorphism: a review. Sedimentology 15, 281–346.

Duval, J.S., 1990. Modern aerial gamma-ray spectrometry and regional potassium map of the conterminous United States. Journal of Geochemical Exploration 39, 249–253.

Eberl, D., Srodon, J., 1988. Ostwald ripening and interparticle-diffraction effects for illite crystals. American Mineralogist 73, 1335–1345.

Eggleston, T.L., Norman, D.I., Chapin, C.E., Savin, S., 1983. Geology, alteration, and genesis of the Luis Lopez manganese district, New Mexico. New Mexico Geological Society Guidebook 34, 241–246.

Elderfield, H., Sholkovitz, E.R., 1987. REE in the pore waters of reducing marine sediments. Earth and Planetary Science Letters 82, 280–288.

Ennis, D.J., 1996. The Effects of K-metasomatism on the Mineralogy and Geochemistry of silicic Ignimbrites near Socorro, New Mexico. New Mexico Institute of Mining and Technology, Socorro.

Glazner, A.F., 1988. Stratigraphy, structure, and potassic alteration of miocene volcanic rocks in the sleeping beauty area, central Mojave Desert, California. Geological Society of America Bulletin 100, 424–435.

Guilbert, J.M., Park, C.F., 1986. The Geology of Ore Deposits. Freeman.

Harrison, W.J., Tempel, R.N., 1993. Diagenetic pathways in sedimentary basins. In: Robinson, A.D.H.a.A.G. (Ed.), Diagenesis and Basin Development. American Association of Petroleum Geologists, pp. 69–86.

Hay, R.L., Guldman, S.G., 1987. Diagenetic alteration of silicic ash in Searles Lake, California. Clays and Clay Minerals 35, 449–457.

Hoch, A.R., Reddy, M.M., Drever, J.I., 1999. Importance of mechanical disaggregation in chemical weathering in a cold alpine environment, San Juan Mountains, Colorado. Geological Society of America Bulletin 111, 304–314.

Hollocher, K., Spencer, J., Ruiz, J., 1994. Composition changes in an ash-flow cooling unit during K-metasomatism, west-central Arizona. Economic Geology 89, 877–888.

Jones, B.F., Weir, A.H., 1983. Clay minerals of Lake Abert, an alkaline saline lake. Clays and Clay Minerals 31, 161–172.

Keller, W.D., 1976. Scan electron micrographs of kaolins collected from diverse environments of origin, I. Clays and Clay Minerals 24, 107–113.

Lasky, S.G., 1932. The ore deposits of Socorro County, New Mexico. New Mexico Bureau of Mines and Mineral Resources Bulletin 8, 139.

Leising, J.F., Tyler, S.W., Miller, W.W., 1995. Convection of saline brines in enclosed lacustrine basins: a mechanism for potassium metasomatism. Geological Society of America Bulletin 107, 1157–1163.

Lindley, J.I., 1985. Potassium metasomatism of cenozoic volcanic rocks near Socorro, New Mexico. Dissertation Thesis, University of North Carolina at Chapel Hill, 563 pp.

May, H.M., Kinniburgh, D.G., Helmke, P.A., Jackson, M.L., 1986. Aqueous dissolution, solubilities and thermodynamic stabilities of common aluminosilicate clay minerals: kaolinite and smectites. Geochimica Cosmochimica Acta 50, 1667–1677.

McBirney, A.R., 1993. In: Igneous Petrology. Freeman, San Francisco, CA, p. 508.

McIntosh, W.C., Sutter, J.F., Chapin, C.E., Kedzie, L.L., 1990. High-precision $^{40}Ar/^{39}Ar$ sanidine geochronology of ignimbrites in the Mogollon–Datil volcanic field, southwestern New Mexico. Bulletin of Volcanology 52, 584–596.

Michard, A., 1988. Rare earth elements systematics of hydrothermal fluids. Geochimica Cosmochimica Acta 53, 745–750.

Nockolds, S.R., Knox, R.W.O.B., Chinner, G.A., 1978. Petrology. Cambridge Univ. Press, Cambridge.

Norman, D.I., Bazrafshan, K., Eggleston, T.L., 1983. Mineralization of the Luis Lopez epithermal manganese deposits in light of fluid inclusion and geologic studies. New Mexico Geological Society Guidebook 34, 247–251.

Norrish, K., Chappell, B.W., 1977. X-ray fluorescence spectrometry. In: Zussman, J. (Ed.), Physical methods in determinative mineralogy. Academic Press, San Diego, CA, pp. 210–272.

Osburn, G.R., 1978. Geology of the eastern Magdalena Mountains, Water Canyon to Pound Ranch, Socorro County, New Mexico. MS Thesis, New Mexico Institute of Mining and Technology, Socorro.

Rehrig, W.A., Shafiquallah, M., Damon, P.E., 1980. Geochronology, geology and listric normal faulting of the Vulture Mountains, Mohave County, Arizona. Arizona Geological Society Digest 12, 89–111.

Roddy, M.S., Reynolds, S.J., Smith, B.M., Ruiz, J., 1988. K-metasomatism and detachment-related mineralization, Harcuvar Mountains, Arizona. Geological Society of America Bulletin 100, 1627–1639.

Shafiquallah, M., Lynch, D.J., Damon, P.E., Peirce, H.W., 1976. Geology, geochronology and geochemistry of the Picacho Peak area, Pinal County, Arizona. Arizona Geological Society Digest 10, 305–324.

Sholkovitz, E.R., 1988. REE in sediments of the north Atlantic Ocean, Amazon delta, and east China Sea: reinterpretation of terrigenous input patterns to the oceans. American Journal of Science 288, 236–281.

Srodon, J., Eberl, D.D., 1984. Illite. In: Bailey, S.W. (Ed.), Reviews in Mineralogy. Mineralogical Society of America, pp. 495–544.

Surdam, R., Parker, R., 1972. Authigenic aluminosilicate minerals

in the tuffaceous rocks of the Green River Formation, Wyoming. Geological Society of America Bulletin 83, 689–700.

Turner, C.E., Fishman, N.S., 1991. Jurassic lake T'oo'dichi': A large alkaline, saline lake, Morrison Formation, eastern Colorado Plateau. Geological Society of America Bulletin 103, 538–558.

Whitney, G., 1990. Role of water in the smectite-to-illite reaction. Clays and Clay Minerals 38, 343–350.

Wintsch, R.P., Kvale, C.M., 1994. Differential mobility of elements in burial diagenesis of siliciclastic rocks. Journal of Sedimentary Research A 64, 349–361.